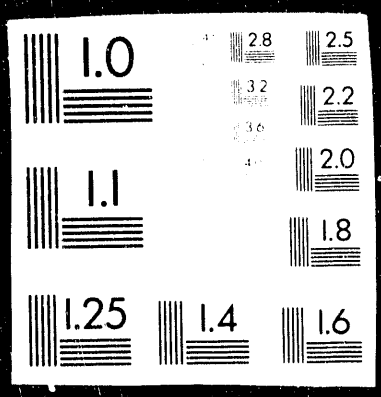

DOE/ER/45416-3

SYNCHROTRON STUDIES OF NARROW BAND MATERIALS

Principal Investigator—J.W. Allen—University of Michigan

Progress Report

7/1/90—6/30/93

DOE/ER/45416--3

DE93 006981

Table of Contents

Not included.

MASTER

I. Progress Report for 7/1/90—6/30/93

A. Overview

Objective and technical approach of the project The objective of this work is to determine the single-particle electronic structure of selected narrow band materials and to analyze the data with a view to elucidating the relation between their electronic structures and novel low energy properties, such as mixed valence, heavy Fermions, the Kondo effect, insulator-metal transitions, non-Fermi liquid behavior or high temperature superconductivity.

We measure the single particle electronic structure of a material using photoemission spectroscopy (PES) and inverse photoemission spectroscopy (IPES). This DoE contract supports PES work at various synchrotrons. These data are combined with data from X-ray photoemission spectroscopy, ultraviolet photoemission spectroscopy, X-ray IPES and Auger spectroscopy, obtained in an in-house laboratory, supported by the NSF. It is very important to have both the synchrotron-excited and the in-house data for a given material. The synchrotron work is of two main types, (1) resonant angle-integrated PES at a variety of photon energies to identify and extract the spectrum of the narrow band electrons of the material, and (2) high resolution, low temperature angle resolved photoemssion spectroscopy (ARPES) to determine the momentum dependence of the hole excitations of a single crystal. These data are analyzed by comparison to theoretical results from both density-functional calculations and from solutions of model many-body Hamiltonians. For the Anderson impurity model, we perform spectral calculations using computer programs obtained from O. Gunnarsson. In any situation where available theory permits, the spectroscopic data is related to the low energy properties of the materials.

Plan and timing of the report This report accompanies a renewal proposal, and the detailed perspective and background for the general issues addressed by the research is given there. At the time of writing, six months of the present grant period remain. The appendix of this report has preprints and reprints, which contain detailed discussion and data figures for the work reported therein. Therefore, for the work reported in papers, no figures are given in this report, and the report discussion is a brief overview. For work not written up yet, data figures are presented and discussed in this report.

Beamtime We have been very successful in competing for beamtime on highly competitive beamlines, as follows.

Wisconsin Synchrotron Radiation Center

1. 1990—3 weeks—Ames-Montana beamline
2. 1991—6 weeks—Ames-Montana beamline
3. 1992—9 weeks—Ames-Montana beamline and facilty beamline
4. 1992—2.5 weeks, Olson PRT time, Sept./Oct.—Ames-Montana beamline
5. 1993—6 weeks scheduled in period through Sept.—Ames-Montana beamline

An application for additional beamtime for the next year period, 1993–1994 will be made.

Brookhaven National Synchrotron Light Source

1. 1991—6 days in period Sept.-Dec.—Dragon beamline
2. 1992—10 days in period May—Dec.—Dragon beamline.
3. 1993—13 days in period Jan-April—Dragon beamline.

An application for additional beamtime in the May to Aug. 1993 period will be made.

Stanford Synchrotron Radiation Laboratory

1. 1993—31 shifts in period Jan-July—Beamline V.

An application for additional beamtime for the next period in 1993 will be made.

B. ZSA systematics and I-M transitions in 3d transition metal oxides

ZSA systematic studied by resonant photoemission at the transition metal 2p edge and the oxygen 1s edge Recently, L.H. Tjeng, while a Bell Labs postdoc working on the NSLS Dragon beamline, reported resonant photoemission studies of the Cu 3d states in CuO using photons at the Cu 2p edge. [L.H. Tjeng et al, Phys. Rev. Lett. **67**, 501 (1991).] He found that the on-off resonance contrast was much larger than for the commonly used resonance at the Cu 3p edge, offering the possibility to extract the 3d emission with the degree of certainty that previously has only been possible in resonant photoemission for rare earth and actinide 4f and 5f states. We made an agreement to collaborate with Tjeng and obtained beamtime for such studies for a range of transition metal (TM) oxides. Very large samples are needed because of the large beam size for this beamline, and we were able to obtain these from the Purdue Materials Preparation Center. Very high quality data were obtained for CoO, MnO, Fe_3O_4, FeO, V_2O_3 and Ti_2O_3. Resonant photoemission was also measured at the O 1s edge. Figs. 1 and 2 summarize the Co 2p and O 1s resonance data for CoO, respectively. Each figure shows the relevant X-ray absorption edge, and valence band spectra taken for photon energies below resonance and on resonance. It is apparent that the 2p resonance has a very large contrast.

One important thrust of the experiments has been to test the systematics of the 3d energy level structure of transition metal compounds as postulated in the Zaanen-Sawatzky-Allen (ZSA) classification scheme, where the early and late transition metal compounds are proposed to be Mott-Hubbard and charge transfer materials, respectively. In the simple ionic picture, these two cases are distinguished by the relative position of the $d^n \rightarrow d^{n-1}$ emission and the O 2p emission. Depending on whether the former has a smaller or larger binding energy than the latter, the material is of the Mott-Hubbard or charge transfer type, respectively. Theoretical analyses indicate that the d^{n-1} emission is the most strongly enhanced at the TM 2p edge. Figs. 3 and 4 show the systematics of the data for the TM 2p and O 1s edges, respectively. In Fig. 3, the off resonance spectra of the early transition metal materials, where the 3d emission is weak, show the oxygen 2p band from – 4 eV to – 10 eV clearly. The on-resonance spectra then show the d^{n-1} emission. At first glance Fig. 3 suggests that the ZSA proposal of a Mott-Hubbard to

charge transfer cross-over as the TM varies from early to late is correct. However the lineshapes of the early TM materials also show a great spreading of weight, including high binding energy satellites outside the oxygen 2p band in addition to the weight at low binding energy above the O 2p band. Our current approach to this data supposes that before hybridization, the $d^n \rightarrow d^{n-1}$ transition lies in the oxygen 2p band for the early TM materials, and that the d-weight both at high and low binding energy has been pushed out of the band by hybridization. Thus these materials are not simple Mott-Hubbard insulators. Theory for this idea is in progress.

Verwey transition in Fe_3O_4 We have also used the resonance effects to study the electronic structure of Fe_3O_4 as it undergoes the Verwey transition at $T_V \sim 120K$, in which there is a large increase in the conductivity as the temperature T is increased through the transition. Fe_3O_4 has two kinds of sites called A and B. The tetrahedral A sites have Fe^{3+} ions and the octahedral B sites have both Fe^{2+} and Fe^{3+} ions. The conductivity jump at T_V is generally understood to involve an order-disorder transition on the B sites. We interpet Fig. 5 as showing that we can distinguish the A-site Fe^{3+} emission centered near – 6 eV from the Fe^{2+} B-site emission near 0 eV. From comparison to that for Fe^{2+} in FeO, the Fe_3O_4 2p absorption edge appears to be a mix of that expected for Fe^{2+} and Fe^{3+} (although we must measure for Fe^{3+} in Fe_2O_3 to check this idea). Consistent with this hypothesis the emission near 0 eV resonantes like Fe^{2+} while the emission near – 6 eV resonates for the part of the absorption curve we interpret at being due to Fe^{3+}. We expect the emission from A site stable Fe^{3+} ions to have the larger binding energy. Fig. 6 shows the conductivity jump at the transition, and emphasizes that in the high temperature conducting phase the conductivity increases with increasing T, in contrast to the decrease usually observed expected for a metal, suggesting an activated conductivity in the high T phase. Consistent with this idea, the high resolution photoemission data of the high T phase shows no Fermi edge. Further work on this system is planned.

$(V_xA_{1-x})_2O_3$ (A=Ti, Cr) Fig. 7 shows the famous and beautiful generalized insulator metal (I-M) transition phase diagram of $(V_xA_{1-x})_2O_3$ (A=Ti, Cr), showing the equivalance of pressure to doping. By varying temperature T in samples with different doping A, we have obtained equally beautiful spectroscopic data for all three of the phases. The variable T data is reproducible under cycling. Considerable effort has been expended in learning the importance of oxygen annealing of the samples, and how to mount and cleave them.

Fig. 8 shows high resolution valence band spectra of pure V_2O_3 in the AFI and PM phases. The data are scaled to the beam flux and the total area is conserved to within 1%. The gap opening in the insulator phase can clearly be seen. Fig. 9 shows the valence band spectra for $(V_{1.988}Cr_{0.012})_2O_3$. For this alloy, varying temperature accesses all three phases of Fig. 7, and indeed all three are seen. The low binding energy PI and AFI phase spectra are very similar to each other and to the AFI spectrum of Fig. 8, as might be expected if the only difference between the two is the presence or absence of AF order. The PM spectrum is similar to its pure V_2O_3 counterpart in Fig. 8, except for a change in relative intensity of the two near E_F peaks. Fig. 10 shows the V 2p (near 512 eV) and O 1s (near 530 eV) XAS spectra for the three phases. The insulator spectra are very similar, and differ in distinct ways from the metallic spectrum. The differences are much more dramatic when the spectra are overlaid on an enlarged scale, and

we expect that modern XAS theories which include multiplet and crystal field splittings may allow these differences to be analyzed. Also difficult to see in this figure is that the oxygen edge shifts slightly between the insulator and the metal, which may reflect the gap opening above E_F. Fig. 11 shows the resonant photoemission spectra in the three phases.

Figs. 12–14 show spectra aimed at learning the nature of the dopant states in the material. Fig. 12 compares the 2p XAS spectrum of Ti doped into V_2O_3 with those of Ti^{3+} and Ti^{4+} standards. It has been surprising to us to learn that Ti takes the formal 4+ valence state when lightly doped into V_2O_3. Fig. 13 shows, in contrast, that Cr 2p XAS spectra imply that Cr as a dopant takes the 3+ valence state, as it does in Cr_2O_3. Fig. 14 shows the resonant photoemission of the Cr 3d states in $(V_{1.988}Cr_{0.012})2O_3$. By comparing to home lab valence band XPS spectra we have taken, we learn that the Cr 3d emission appears at essentially the same energy relative to the oxygen bands as it does in Cr_2O_3, as might be expected from the XAS results, and from the highly insulating character of Cr_2O_3.

These data contain an enormous amount of new information on the electronic structure of this important alloy system. This report has contented itself with simply presenting some of the data. We are presently considering the interpretation of the data in the light of our new thinking about the early TM materials, and of the several previous electronic structure models put forth for this system and for its MI transition.

C. Insulator-metal transitions in superconducting cuprates

$Nd_{2-x}Ce_xCuO_4$ The two systems $Nd_{2-x}Ce_xCuO_4$ and $La_{2-x}Sr_xCuO_4$ are thought to be electron and hole doped, respectively. In our previous angle integrated photoemission studies on these materials [J.W. Allen et al, Phys. Rev. Lett. **64**, 595 (1990)] we found that E_F for the metals occurs in new spectral weight in the gap of the insulator and that E_F is in roughly the same position for both systems so that it does not "jump the gap" as one switches from hole to electron doping. Recently X-ray absorption spectroscopy (XAS) studies [H. Romberg et al, Phys. Rev. B **42**, 8768 (1990) and C.T. Chen et al, Phys. Rev. Lett. **67**, 1918 (1991)] at the oxygen 1s edge have been interpreted as showing that for hole doping E_F lies in the insulator valence band and that for electron doping E_F lies in the insulator conduction band. The fact that E_F is observed directly in photoemission but must be inferred after data interpretation in XAS strongly favors the photoemission result on this question, but the greater surface sensitivity of photoemision relative to XAS has been cited as a reason to ignore the photoemission results. Also, since sample variability is well known in these materials, it is possible that the data disagree because they were taken on different samples. We have studied this question further in $Nd_{2-x}Ce_xCuO_4$ in two ways.

First, we have repeated our angle integrated studies, including at the same time O 1s XAS performed by the yield method. We find that the photoemission data are the same as previously, and that the XAS data also agree with those of other workers, so the conflict does not have its origin in sample differences for this material. The photoemission data are reported in Pub. 11 and the XAS data are shown in Fig. 15. The upper two solid and dotted curves in the figure compare data taken by Krol et al [Phys. Rev. B **42**, 4763 (1990)] in the absorption mode with our

data, respectively, showing they are the same. We also have a complete set of core level spectra taken in the home lab and are currently searching for a unified interpretation of all the data.

Second, we have made angle integrated and angle-resolved studies of single crystals with x=0, 0.1 and 0.15. The former confirm our results for growth of spectral weight in the insulator gap, and the latter show, for x=0.15, k-dependent excitations which define a Fermi surface in good agreement with band calculations, i.e., satisfying the Luttinger theorem. The finding of a Luttinger Fermi surface in the material is very significant because (1) it is the first such instance for an electron doped material; (2) it is the first such instance for a material with the simple paradigm electronic structure which requires alloying to drive it metallic; (3) it adduces to the gap spectral weight the same credibility as is given to the near E_F weight in $Bi_2Sr_2CaCu_2O_8$ and $YBa_2Cu_3O_7$, where Luttinger Fermi surfaces are also seen; (4) it shows that the gap spectral weight is not an impurity band; (5) it completes for $Nd_{2-x}Ce_xCuO_4$ the experimental proof of the scenario we put forth previously for the metal insulator transition in the superconducting cuprates. This work has been submitted to Phys. Rev. Letters. [Pub. 11] We also acknowledge here that similar angle-resolved data has been obtained by King et al at Stanford.

$La_{2-x}Sr_xCuO_4$ It is obviously of great importance for the picture we are developing to have data for $La_{2-x}Sr_xCuO_4$ equivalant to that now obtained for $Nd_{2-x}Ce_xCuO_4$. Thus far the data from both ceramic and single crystal samples do not vary systematically with x, causing us to mistrust the data taken to date. We will continue studies of this system as new samples become available.

$Y_{1-x}Pr_xBa_2Cu_3O_7$ Pr in this system acts initially to quench superconductivity. It is exceptional in this respect because other rare earths doped into this system, except for Ce and Tb, which have the drastic effect of inducing a new crystal structure, have no effect on the superconductivity. For large enough x, the material then becomes an insulator. One can speculate that an understanding of this behavior will impact the understanding of the electronic structure of the Cu-O planes. Dating from before the beginning of this grant, we have devoted much effort to performing electron spectroscopy on this system. Along with many other workers, our results indicate that the Pr valence is close to 3+. A surprising result is that the Pr 4f spectrum obtained by resonant photoemission does not appear to display the Fermi edge in metallic samples, but to go to zero at E_F. However, we have found it difficult to obtain reproducible results on several series of ceramic samples. These typically show a fairly large valence band 9eV peak, commonly thought to indicate a spurious contribution to the spectrum, and also multiple peaks in the oxygen 1s core level photoemission spectrum. For this reason we have not trusted our data.

Most recently we have obtained from our UCSD collaborators single crystals with small x in the metallic range, and have made preliminary angle integrated resonant photoemission studies. These studies again show that the 4f emission has gone to zero as it approaches E_F. We will continue the single crystal work.

D. Fermi liquid and non-Fermi liquid behavior in ARPES lineshapes

$Bi_2Sr_2BaCu_2O_8$ photoemission lineshape analysis The angle resolved photoemission spectroscopy (ARPES) spectral lineshapes of $Bi_2Sr_2BaCu_2O_8$, very near the Fermi energy E_F in the normal state, have been taken as evidence for non-Fermi liquid behavior in this material. Following up this idea, we have fit ARPES spectra of $Bi_2Sr_2BaCu_2O_8$ taken by Olson et al using normal and marginal Fermi liquid self-energies. Both theories fit the data equally well provided a sufficiently large inelastic background is included. However, the required backgrounds are, respectively, 60 and 15 times larger than that given by usual background subtraction procedures. A paper on this work has been published in the proceedings of a Fermiology Workshop held at Argonne National Laboratory in March, 1991. [Pub. 1]

1T-$TiTe_2$ ARPES In our lineshape fitting effort on $Bi_2Sr_2BaCu_2O_8$ (preceding subtopic) the need to calibrate ARPES for Fermi liquid materials became obvious. We have selected the quasi two-dimensional material $TiTe_2$ for this purpose and have taken detailed low temperature high resolution ARPES data for a nondegenerate band crossing E_F. The data are of very high quality, and we have analysed them using both the Fermi liquid and the marginal Fermi liquid lineshapes to see if the data can distinguish the two theories, and it appears that they definitely favor the Fermi liquid. The work has been published in Phys. Rev. Lett. [Pub. 5] and a detailed paper is in preparation. We have also begun to study the effects of variable temperature and disorder induced by sputtering. The data are shown in Figs. 16 and 17. The main part of each figure shows spectra normalized to the beam flux, and the inset shows spectra normalized at the peak heights. The inset shows the expected broadening effects, but it is then somewhat surprising that the data normalized to the beam flux shows decreasing peak intensity, but essentially no change in the inelastic part of the spectrum near 300 meV binding energy. We might expect that the broadening and intensity loss implies inelastic scattering which would increase the inelastic background. Further studies of this type are planned in the hope that we can better understand inelastic backgrounds in PES.

E. Heavy-Fermion and non–Fermi liquid 5f electron systems

$A_{1-x}U_xPd_3$ (A=Y, Th, Zr) Our studies of $U_xY_{1-x}Pd_3$ are now complete and analyzed. The data consist of synchrotron-excited resonant photoemission for the U5f states, combined with U-M lab photoemission data on the valence band and core levels and BIS data for the conduction band 5f states. The data are correlated with transport measurements performed by our collaborators, the Maple group at U.Cal. San Diego (UCSD) and interpreted as showing that the Fermi energy E_F shifts to lower enery with decreasing x as Y^{3+}replaces U^{4+}. Accompanying this, for $x < 0.3$, the transport properties show the Kondo effect, and the BIS spectrum develops a Kondo resonance. Very exciting is the finding that the Kondo effect in this system has novel properties, such as a residual ground state entropy, which display non-Fermi liquid behavior probably due to an underlying two-channel quadrupolar Kondo effect at the single ion level. Separate PRL's on the transport and spectroscopy have been published [Pubs 2, 3, and 6] , and two invited talks have been given.

Following up this work, we have also made resonant photoemission measurements on polycrystalline samples of $Zr_{1-x}U_xPd_3$ and $Th_{1-x}U_xPd_3$. [Pub. 9] We expect Zr and Th to have the 4+ valence states, so that E_F will not shift. For both systems this behavior is observed, although for Zr the spectrosocpy is complicated by surface segregation effects. The UCSD transport data is also consistent with these results. By using Th to control the E_F position, one can compare two samples with different U concentrations but the same E_F. UCSD transport measurements show that the Fermi level tuning effect, and not the variation of inter-site interactions associated with variation of the concentration, is by far the dominant effect.

URu_2Si_2 We have analyzed our low temperature high-resolution ARPES data for single crystals of the heavy-fermion material URu_2Si_2. We have compared the results to band theory to the extent possible. Our normal emission data with varible photon energy $h\nu$, probing the Γ to Z direction, show little dispersion. Instead, the spectral peaks occur at energies where the Γ to Z band structure implies peaks in the one-dimensional density of states for this direction. In contrast, data taken with fixed photon energy and variable angle away from normal emission show dispersing features. Following other workers, we tentatively understand this to imply a large uncertainty in momentum perpendicular to the surface, due to a small mean free path, and a continued conservation of momentum parallel to the surface. A detailed paper describing this work has been submitted to the Physical Review [Pub. 10].

$YbAl_3$ Yb is the one-hole analog to Ce, and so the Kondo resonance in Yb materials appears in the photoemission spectrum, where its lineshape and temperature dependence can be studied with high resolution. We have measured the 4f lineshape at 20K in $YbAl_3$ at the SRC Ames-Montana beamline, and, with L.H. Tjeng and S.-J. Oh, have measured the temperature dependence of the lineshape on the NSLS Dragon beamline. We find results in agreement with predictions of the impurity Anderson model, in contradiction to findings by Joyce and Arko [private communication and Bul. Am. Phys. Soc. **37**, 637 (1992)] who find broad lines with no T-dependence. Our lineshape study is reported in Pub. 8 and our T-dependent data are shown in Figs. 18 and 19. These data will be written up for Phys. Rev. Letters in the very near future, and reported at the 1993 March APS meeting. Further studies, including joint experiments with Joyce and Arko are planned.

Ce materials Joyce, Arko, and coworkers have recently reported data the 4f spectra of low T_K cerium materials, such as $CeSi_2$, which they intepret as invalidating the use of the impurity Anderson model for analyzing such spectra. [J.J Joyce et al, Phys. Rev. Lett. **68**, 1992). Gunnarson and the P.I. have written a rebuttal [Pub. 7] pointing out some aspect of the theory as it applies to Ce spectra which, in our experience, have helped to explain some of the problems discussed by Joyce and Arko. As a further effort to understand these issues, we are now engaged, with former student Lizhong Liu (now a postdoc at Yale), in a detailed analysis of both published and our own electron spectrosocpy data for $CeSi_2$, using the impurity Anderson model and matrix elements calculated with the LDA. The first results of this work will be reported at the 1993 March APS meeting.

We have also made X-ray magnetic circular dichroism (XMCD) measurements at the Fe 2p and Ce 3d edges to detect the presence of magnetic moments in the ferromagnetic material

$CeFe_2$. The spectroscopic properties of this interesting material show that the single-site Kondo temperature of the Ce ions is of order 1000K, much higher than the ferromagnetic transition temperature. Nonetheless we find evidence of a magnetic moment on the Ce sites, in addition to the expected one on the Fe sites. This result is consistent with the idea of the ferromagnetic state developing in the quasiparticles of a Kondo Fermi liquid established at much higher temperatures. This is the first XMCD study of a Kondo lattice system, and the results will be reported at the 1993 March APS meeting.

F. Kondo insulators

We have begun high resolution studies on a group of small-gap insulating materials. In the mid-70's, these materials, such as SmB_6, were known as mixed valent hybridization gap systems. Recently new materials of this type have been discovered, and it has been realized that the energy gaps are probably related to a small energy scale of the kind involved in the Kondo effect. Thus these materials have a new name—the Kondo insulators, and they now enjoy a revival of theoretical and experimental interest. It appears likely that in these small gap materials a normal size gap insulator is lurking in the background. In the case of cerium based compounds this would be a tetravalent Ce material. Thus far we have taken data on $CeFe_4P_{12}$ and $PrFe_4P_{12}$. The former is thought to be a Kondo insulator, presumably with Ce mixed valent, and the latter, for contrast, is a metal. These data will be combined with U-M lab data directed at learning the valence of Ce in this material.

It is an interesting question whether the insulating state of $Y_{1-x}Pr_xBa_2Cu_3O_7$ should be regarded as a Kondo insulator. From the activation energy of the insulator's resistivity one infers a very small gap, much less that typical charge transfer gaps. Thus it seems likely that another mechanism, intimately involving the Pr 4f states, is probably at work. One can speculate that the charge transfer insulator is the normal sized gap material lurking in the background of this material. Thus our work on this system is also part of our Kondo insulator studies. However, there may also be some extra consequences of the involvement of the Cu-O planes.

II. List of Figures

Co 2p(3/2) Resonance Valence Spectra

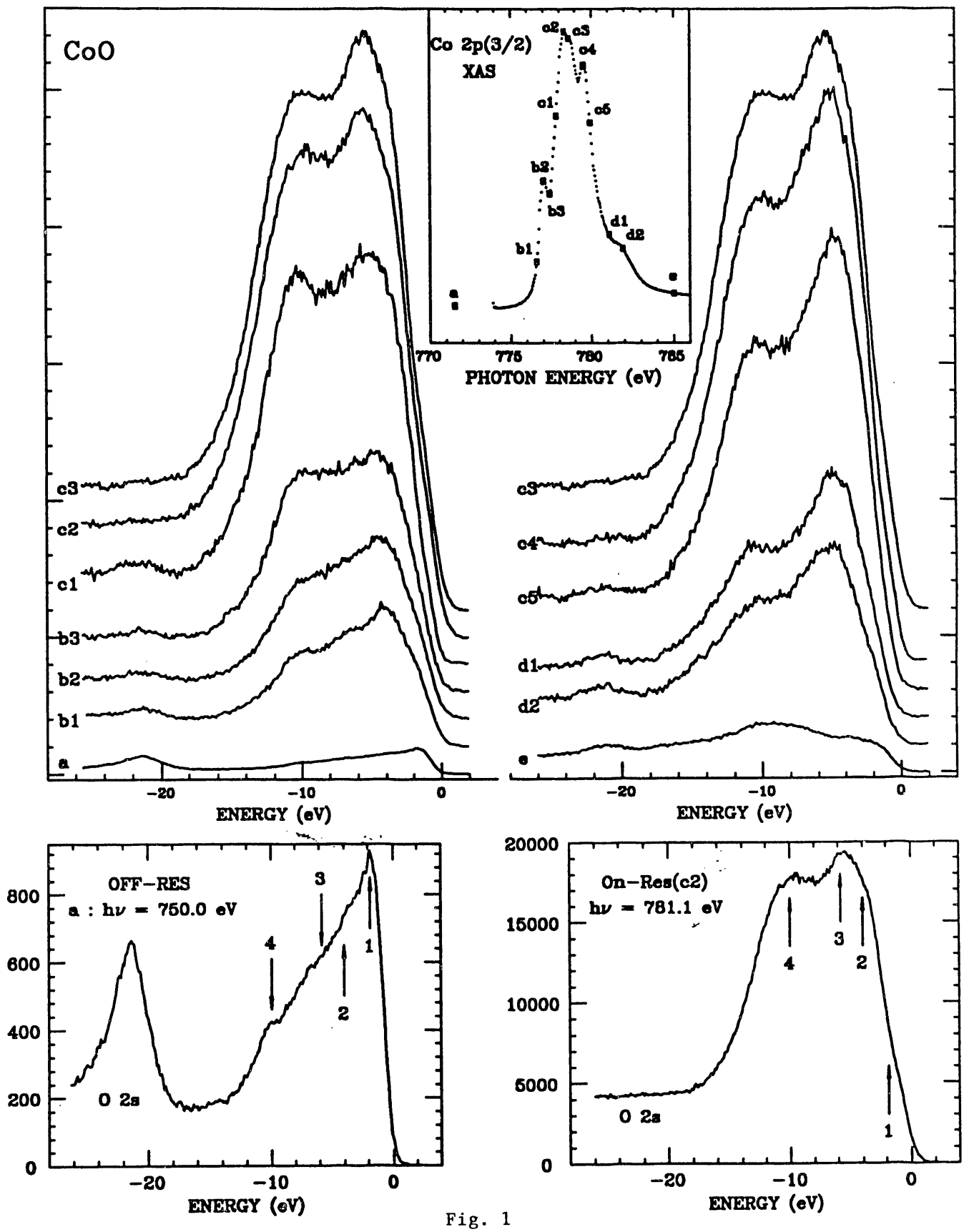

Fig. 1

O 1s Resonance Valence Spectra

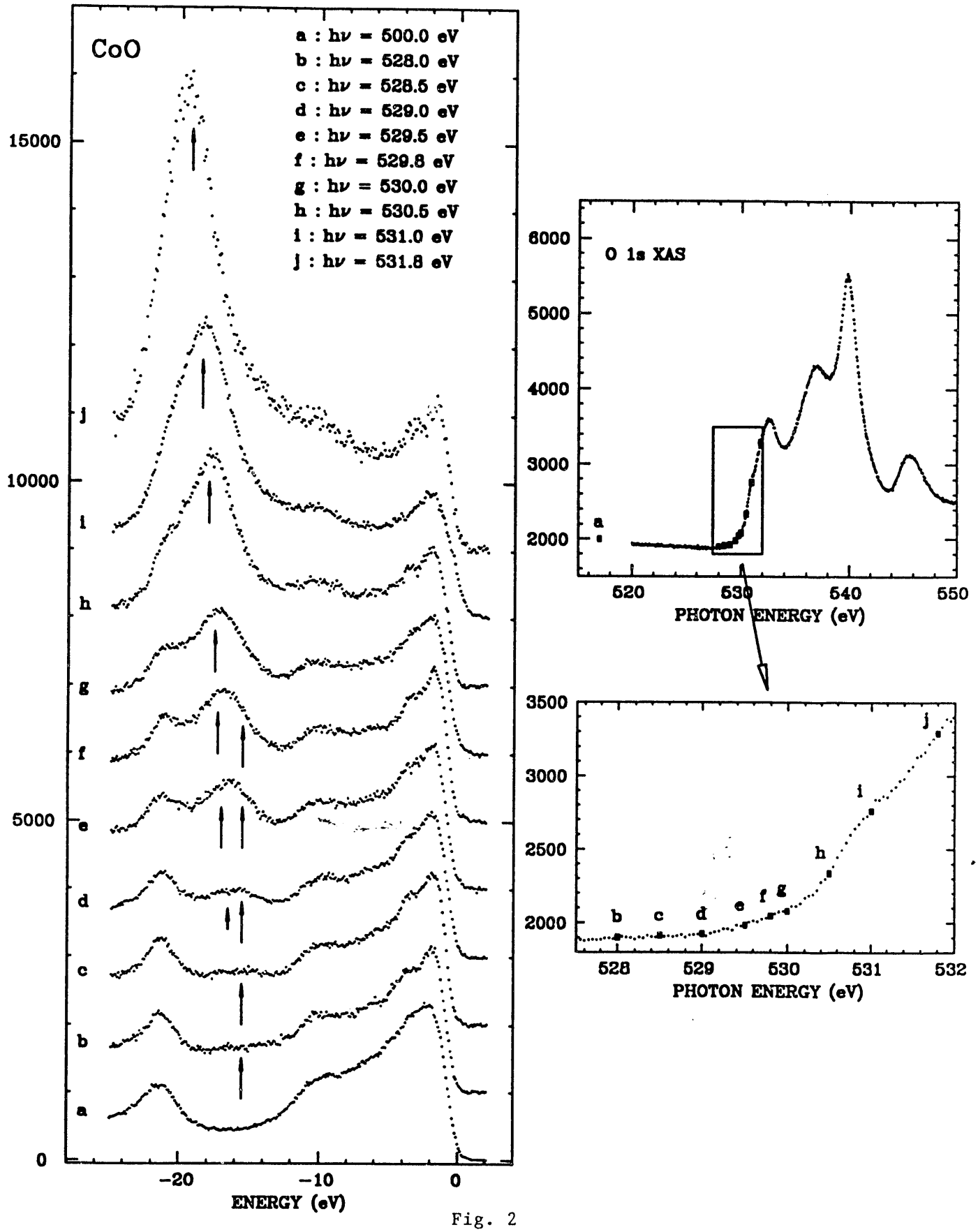

Fig. 2

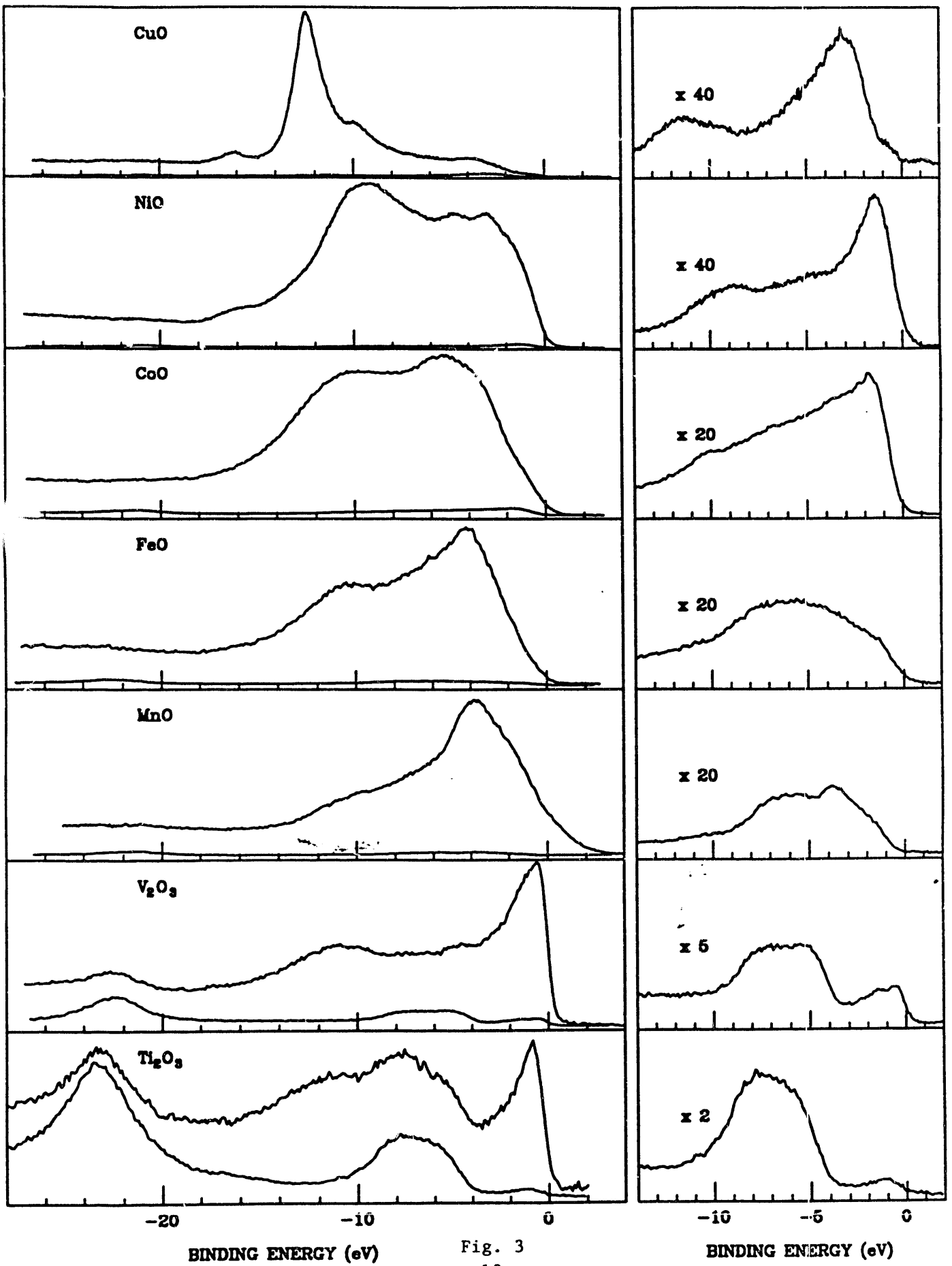
TM 2p On and Off RESPES
Off-Resonance
CuO
NiO
CoO
FeO
MnO
V_2O_3
Ti_2O_3
x 40
x 40
x 20
x 20
x 20
x 5
x 2
-20
-10
0
-10
-5
0
BINDING ENERGY (eV)
BINDING ENERGY (eV)

Fig. 3

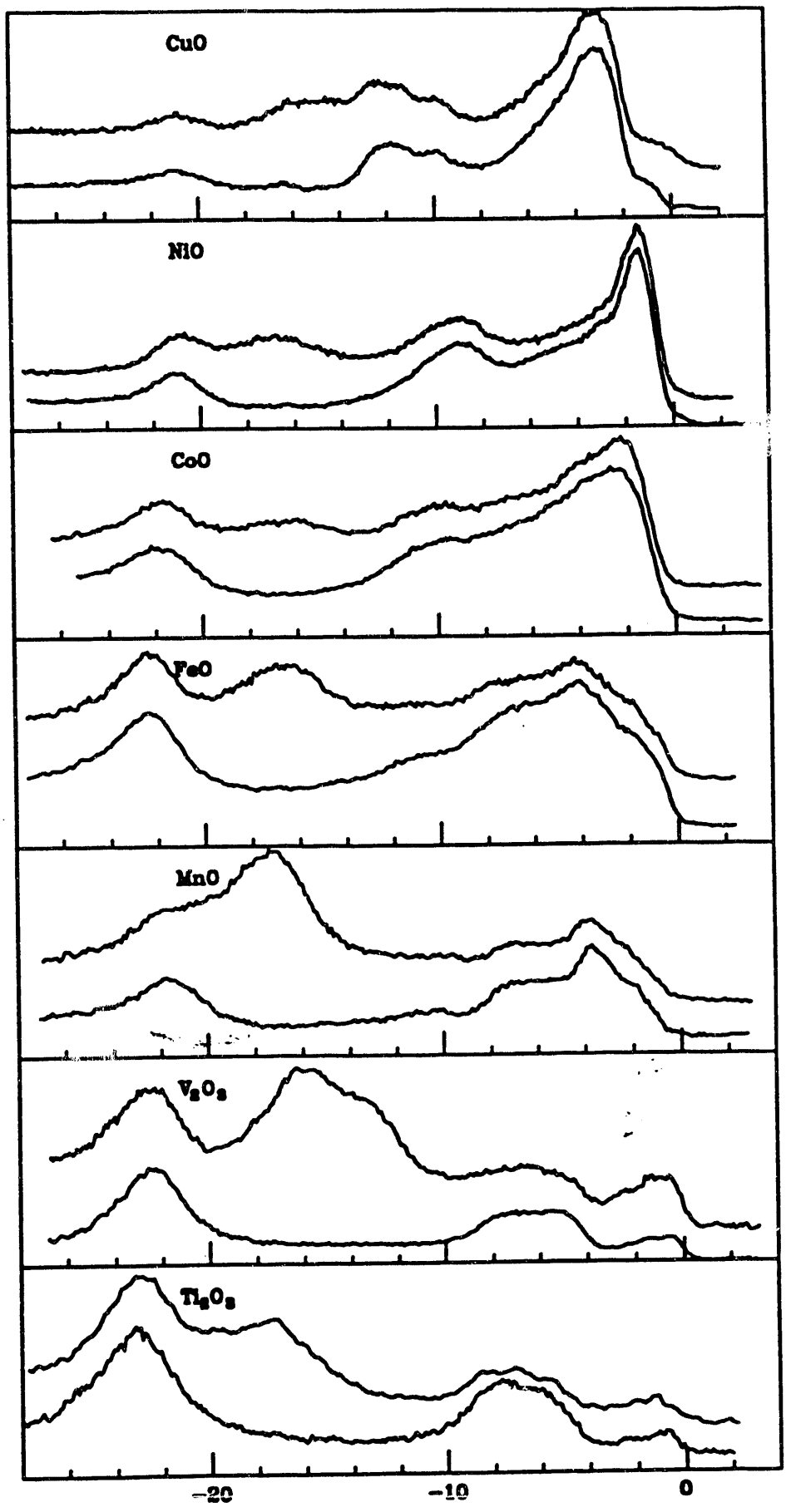
O 1s On and Off RESPES
CuO
NiO
CoO
FeO
MnO
V_2O_3
Ti_2O_3
-20
-10
0
BINDING ENERGY (eV)

Fig. 4

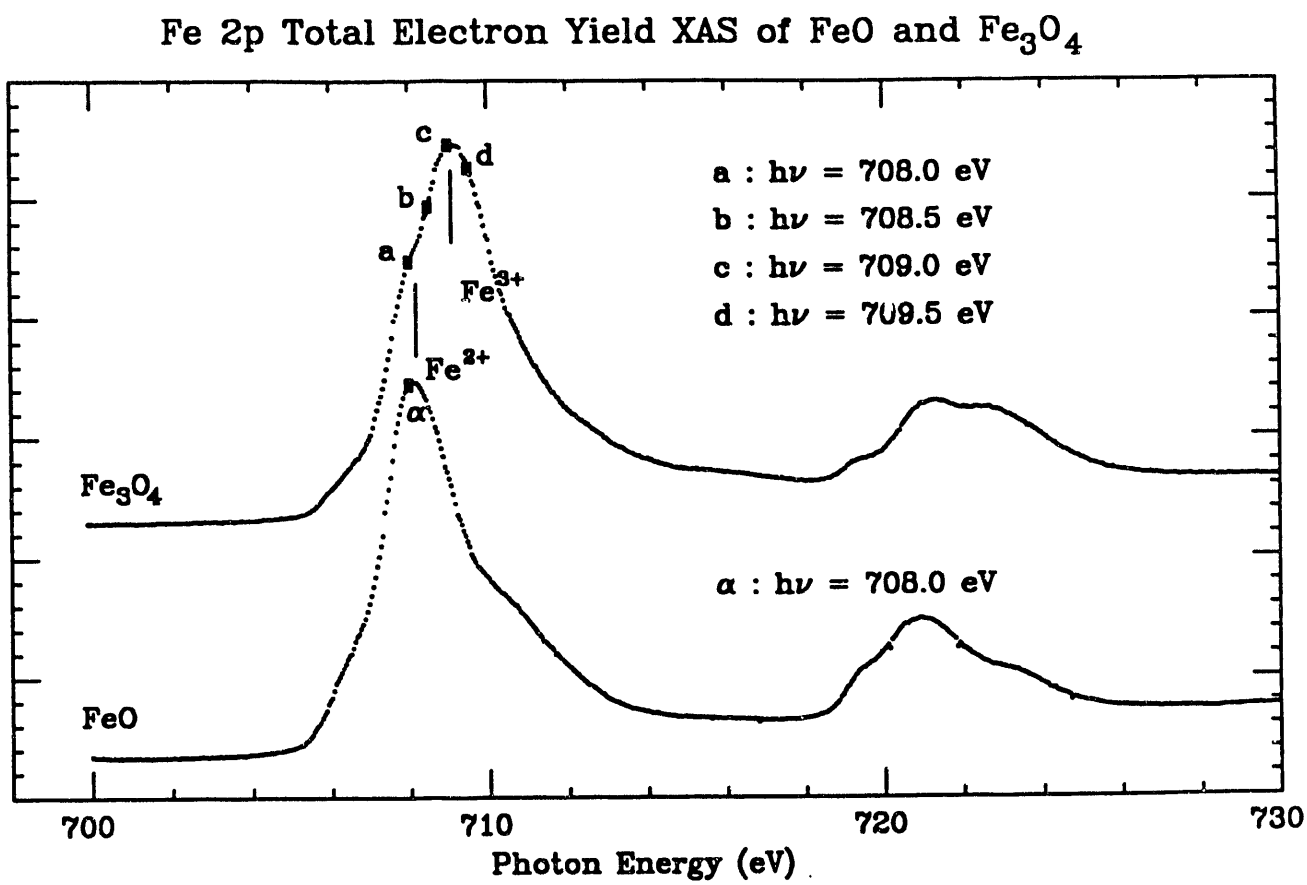
Fe 2p Total Electron Yield XAS of FeO and Fe_3O_4
a : hν = 708.0 eV
b : hν = 708.5 eV
c : hν = 709.0 eV
d : hν = 709.5 eV
α : hν = 708.0 eV
Fe_3O_4
FeO
Fe^{3+}
Fe^{2+}
700
710
720
730
Photon Energy (eV)

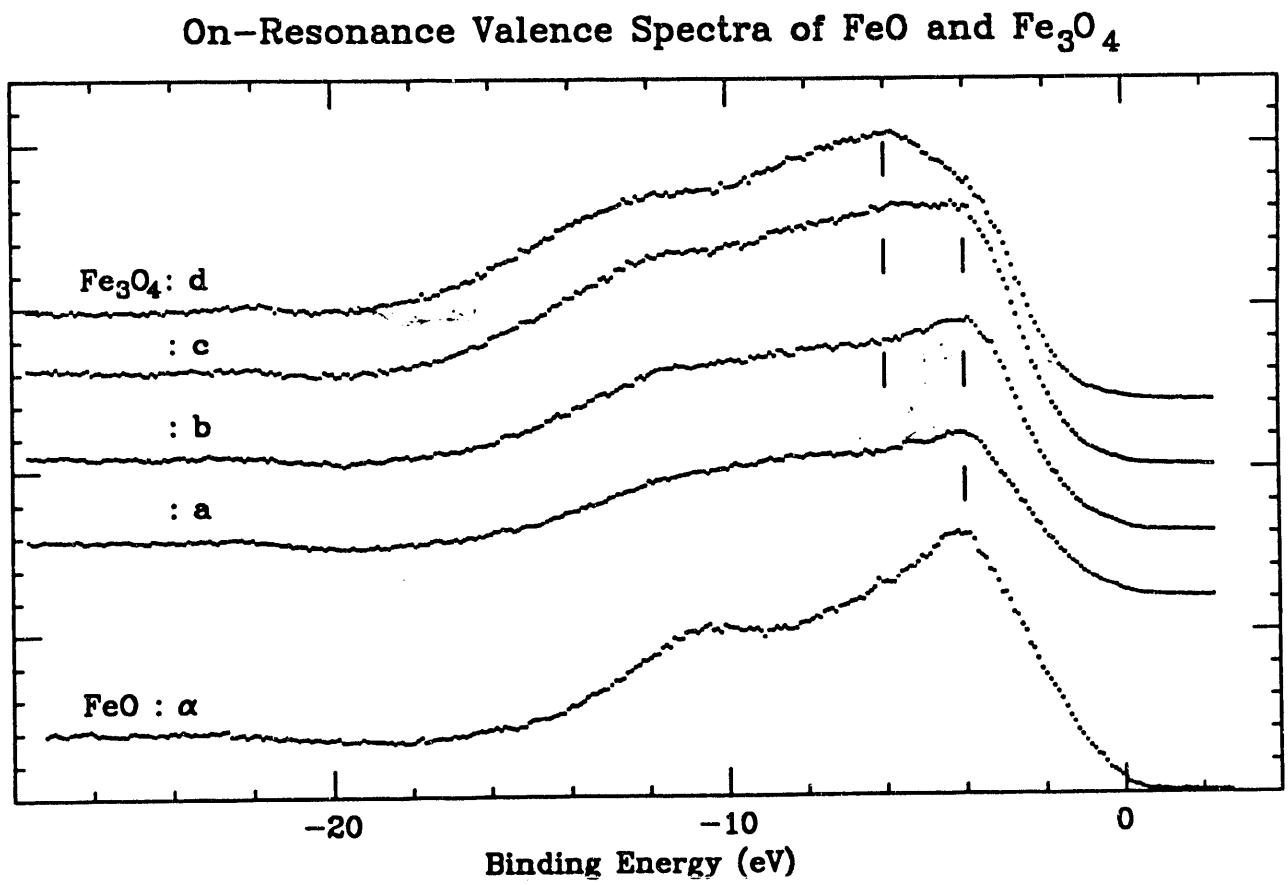
On-Resonance Valence Spectra of FeO and Fe_3O_4
Fe_3O_4: d
: c
: b
: a
FeO : α
−20
−10
0
Binding Energy (eV)

Fig. 5

Valence Band Spectrum above Tv

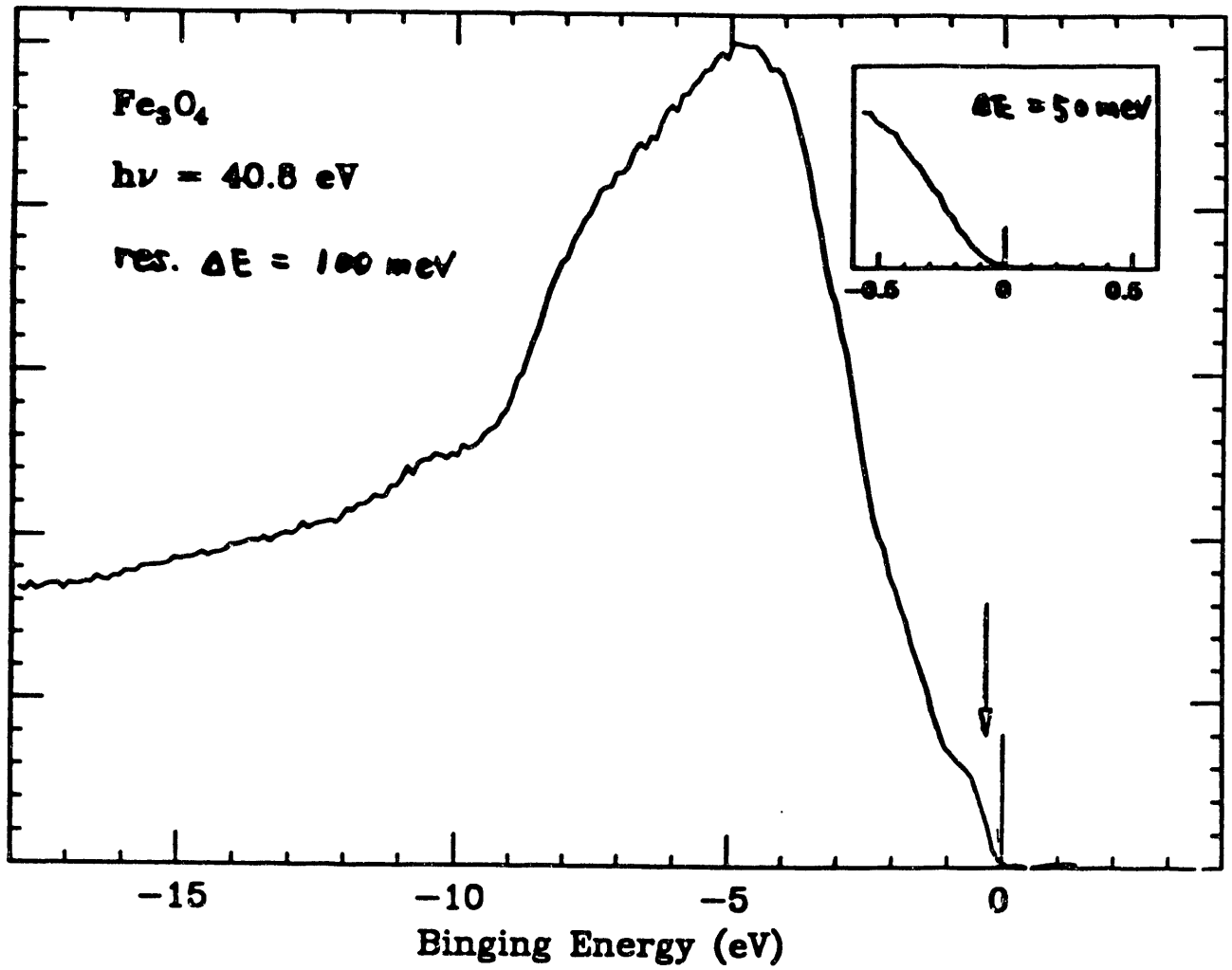

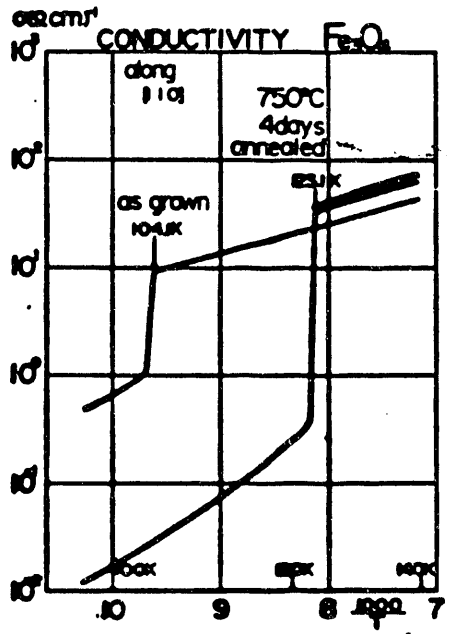

Conductivity increases with increasing Temperature.

⇒ Unusual in Normal Metals

Fig. 6

Generalized Phase Diagram of V_2O_3

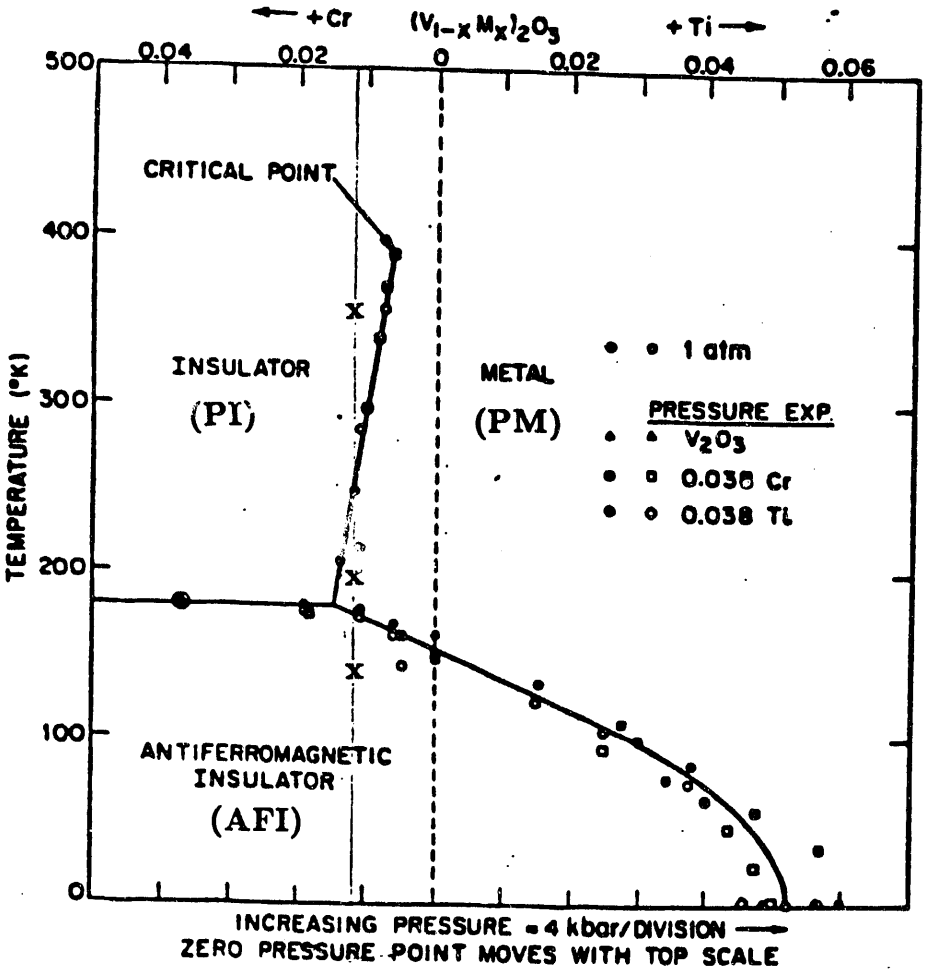

(McWhan et al, PRB 7, 1920 (1973))

Fig. 7

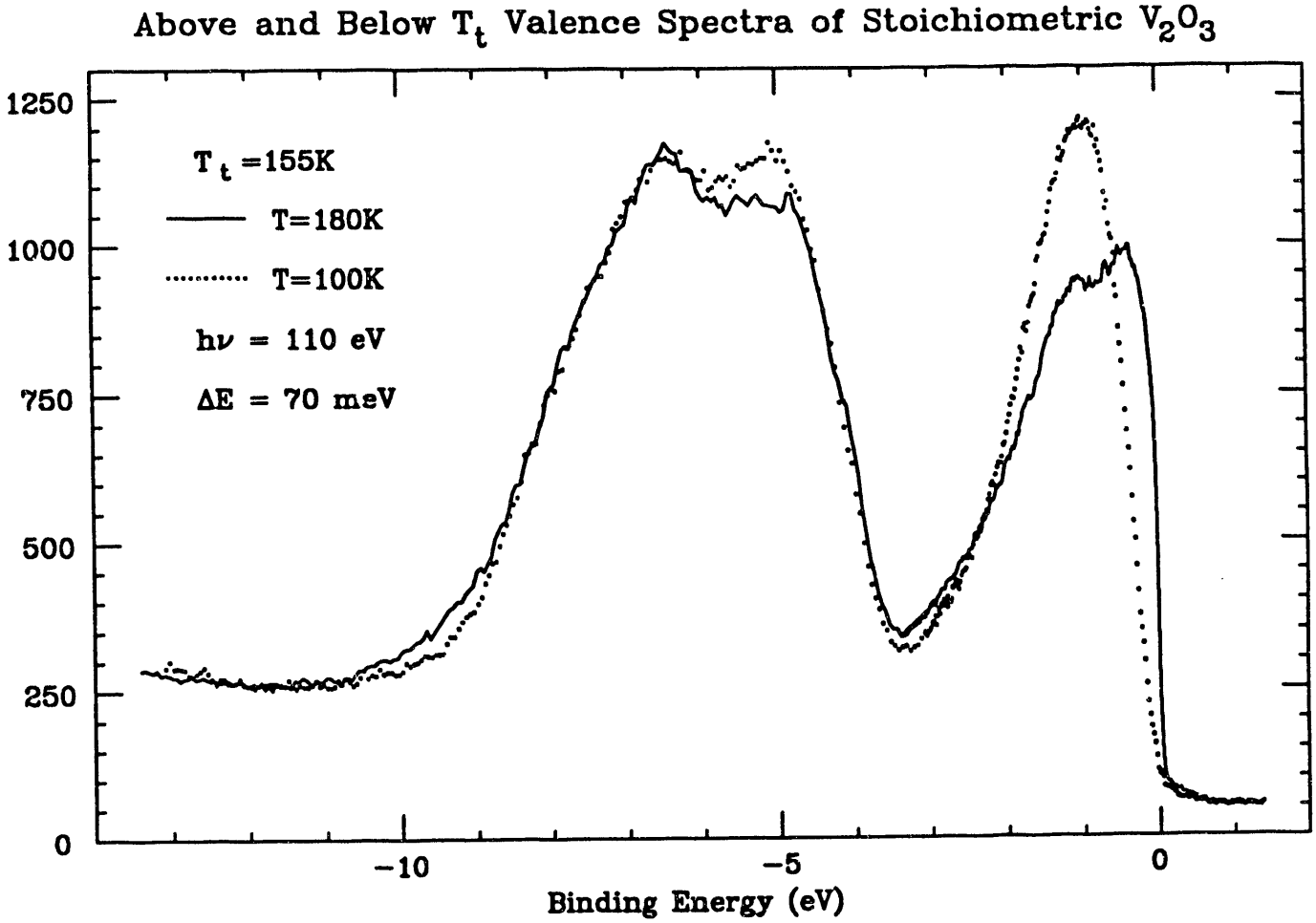
Above and Below T_t Valence Spectra of Stoichiometric V_2O_3
T_t =155K
T=180K
T=100K
hν = 110 eV
ΔE = 70 meV
1250
1000
750
500
250
0
−10
−5
0
Binding Energy (eV)

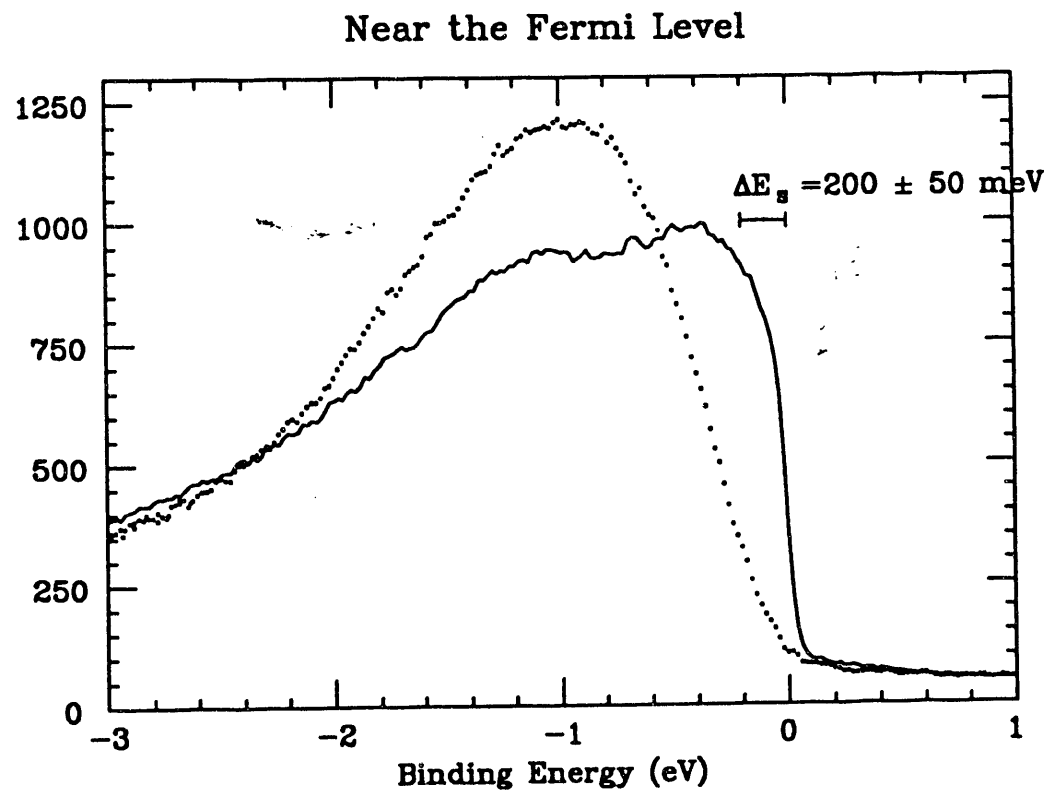
Near the Fermi Level
ΔE_s =200 ± 50 meV
1250
1000
750
500
250
0
−3
−2
−1
0
1
Binding Energy (eV)

Fig. 8

Hi-Resolution Valence Band Spectra for $(V_{1.988}Cr_{0.012})_2O_3$

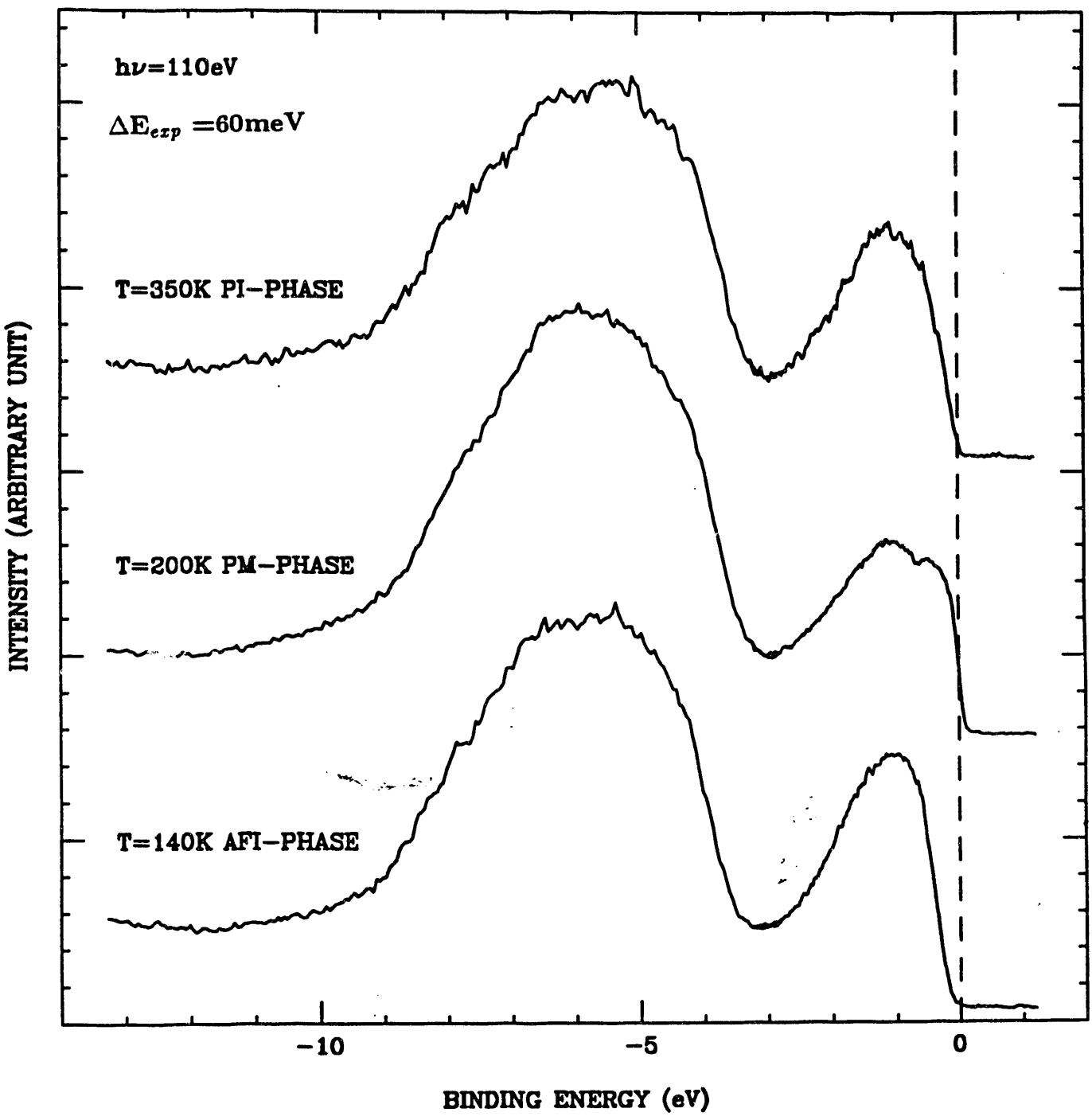

Fig. 9

X-ray Absoption Spectra for $(V_{1.988}Cr_{0.012})_2O_3$

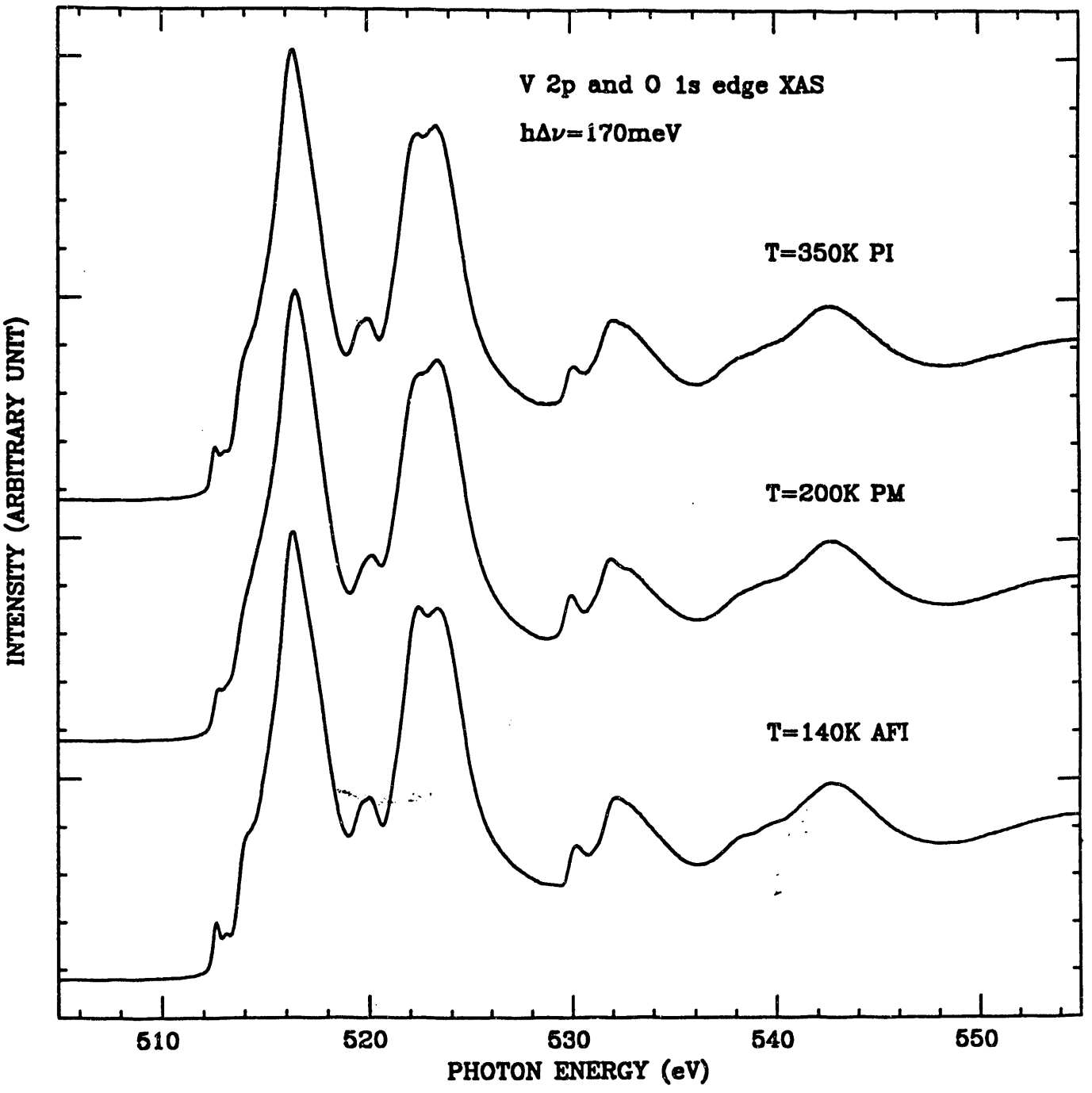

Fig. 10

On- and Off- Resonant Valence Band Spectra at V 2p edge

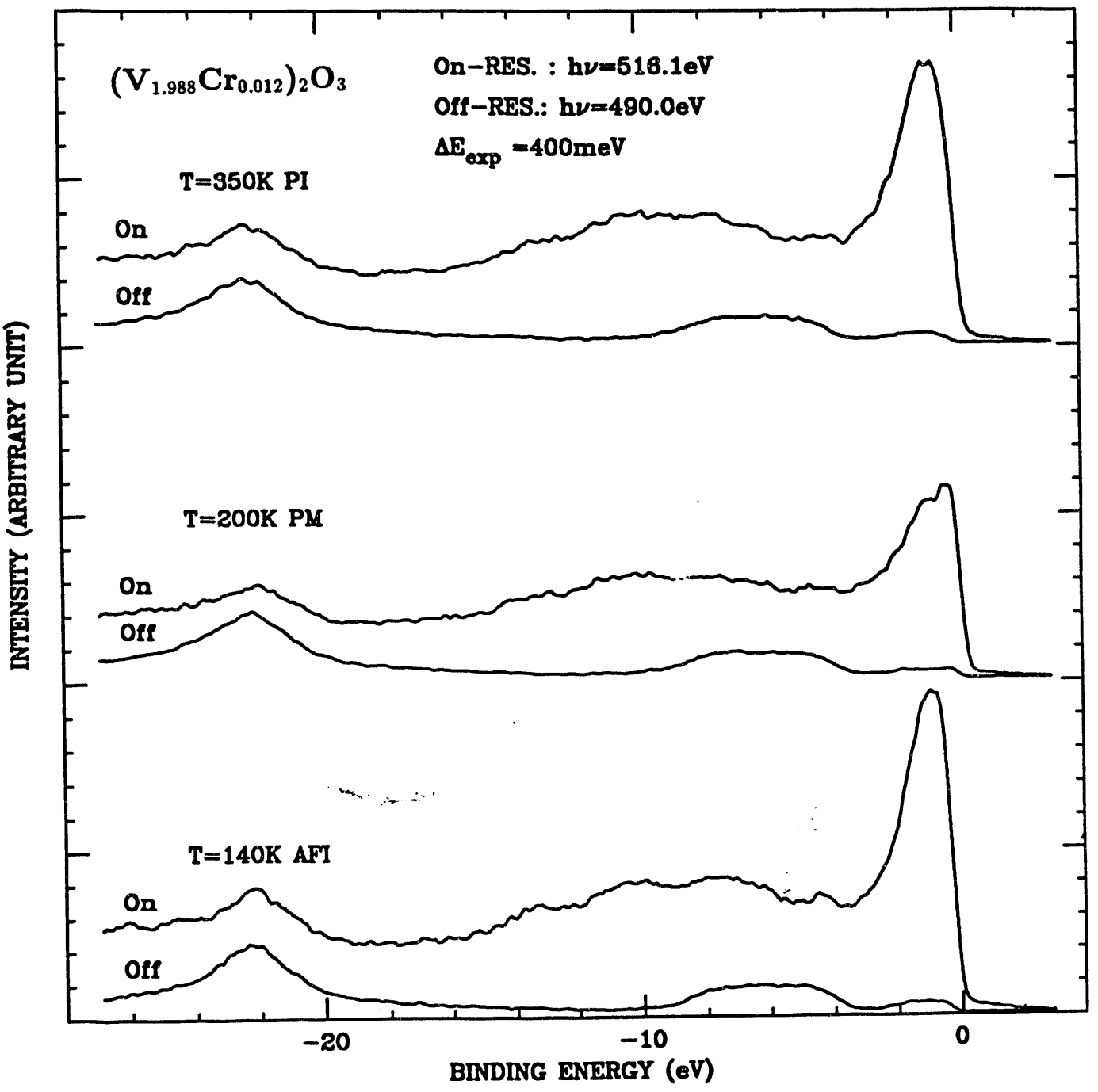

Fig. 11

Ti 2p X-ray Absoprtion Spectra

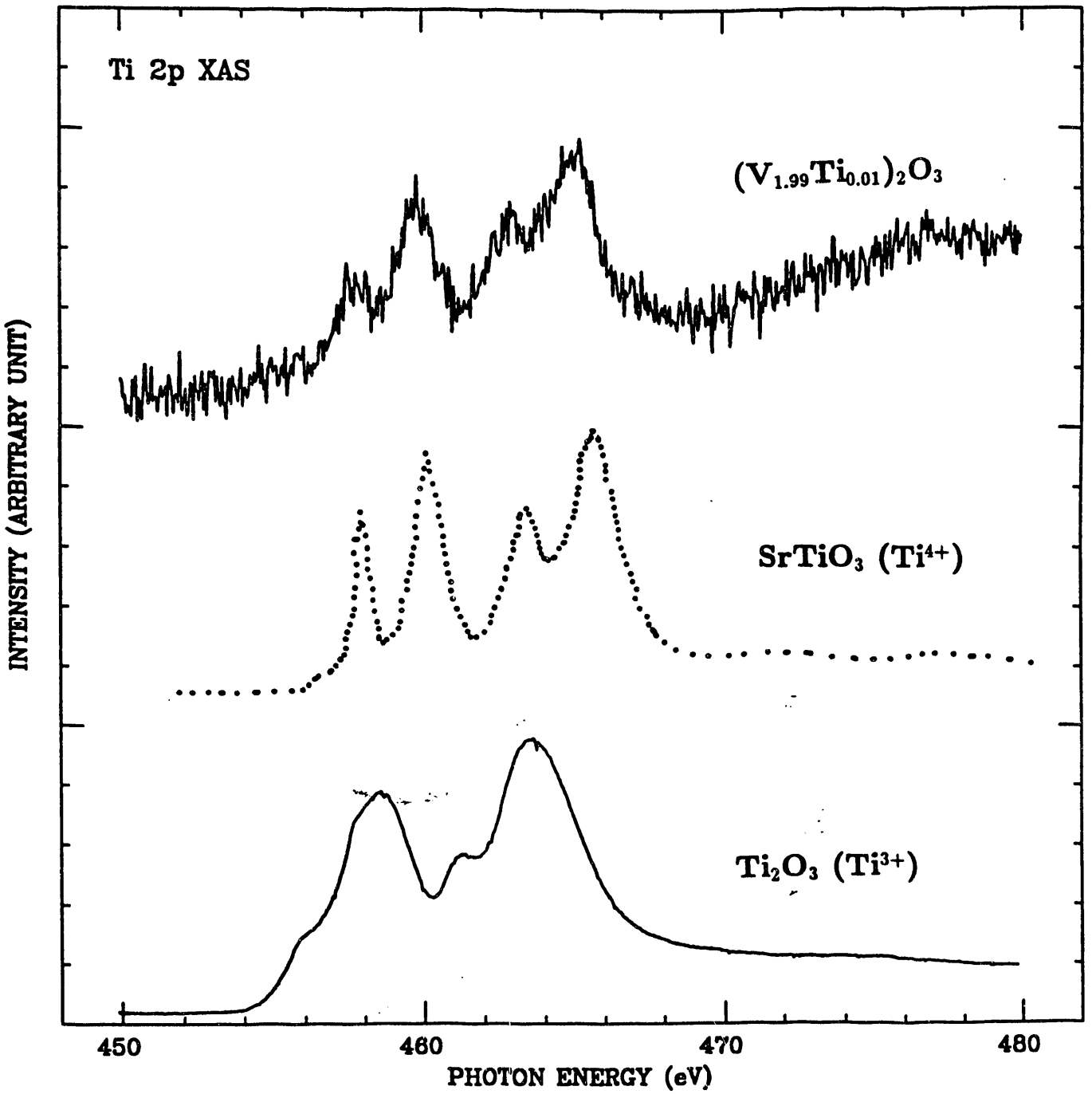

Fig. 12

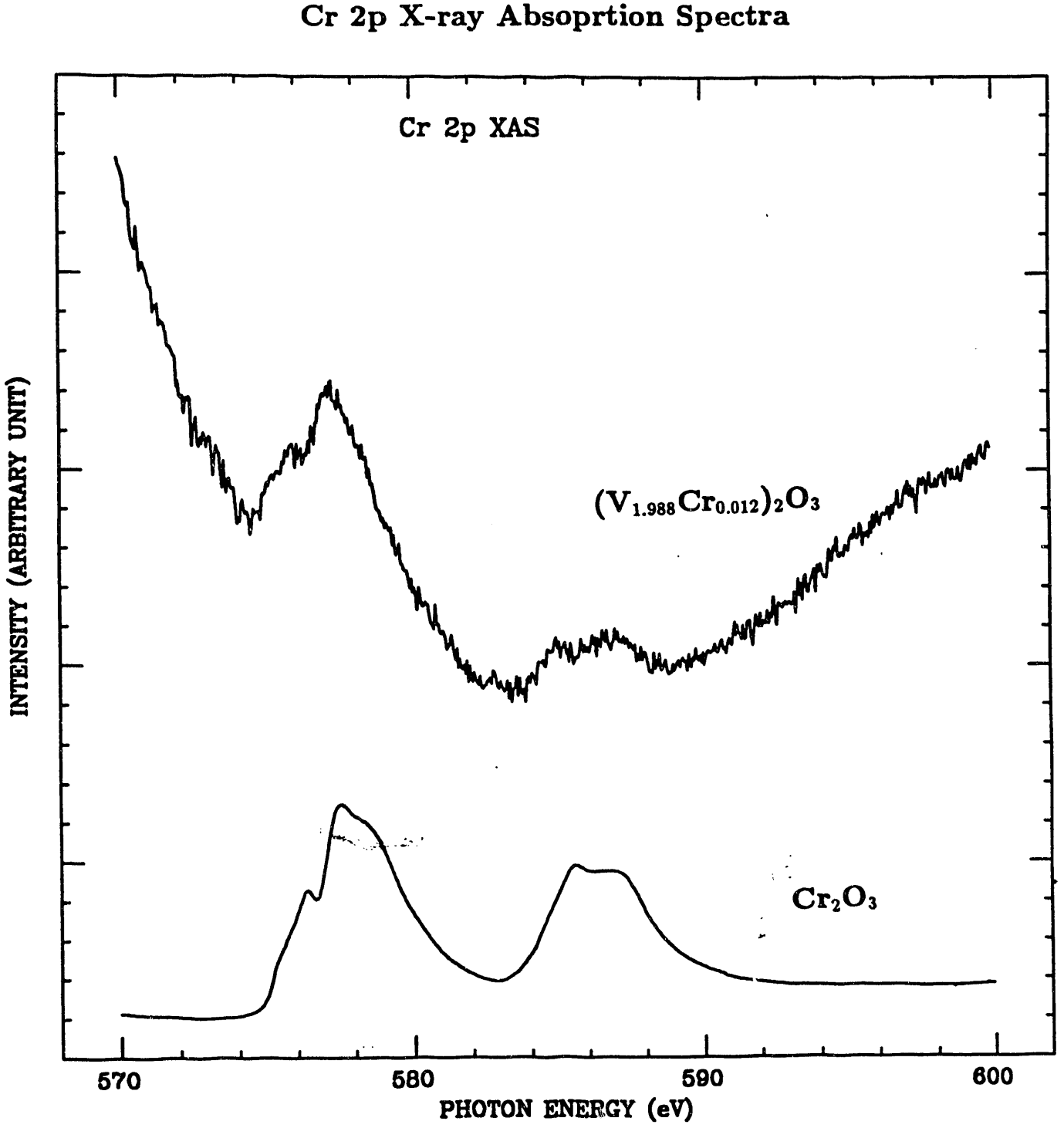
Cr 2p X-ray Absoprtion Spectra
Cr 2p XAS
INTENSITY (ARBITRARY UNIT)
$(V_{1.988}Cr_{0.012})_2O_3$
Cr_2O_3
570
580
590
600
PHOTON ENERGY (eV)

Fig. 13

On- and Off- Resonant Valence Band Spectra at Cr 2p edge

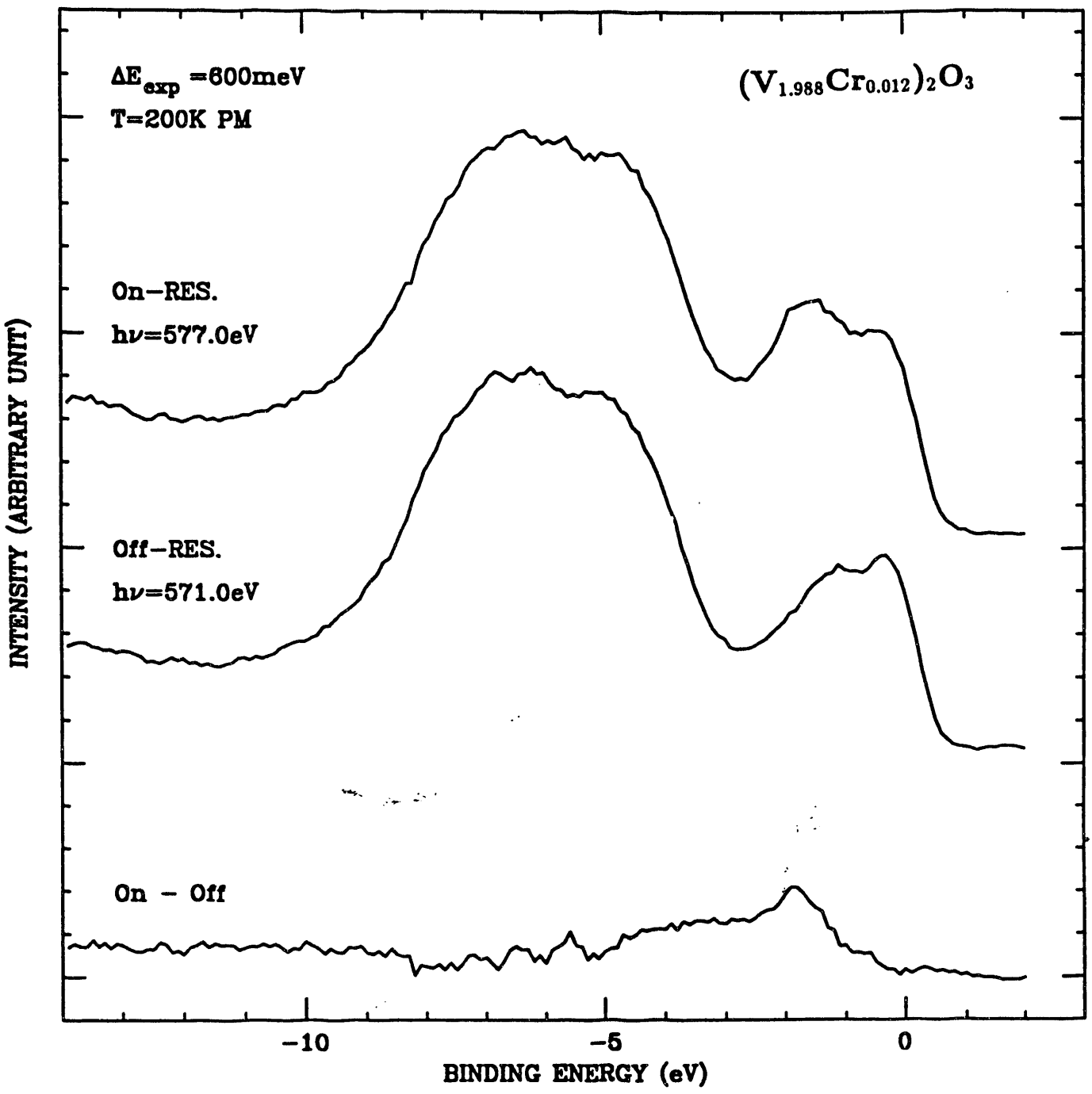

Fig. 14

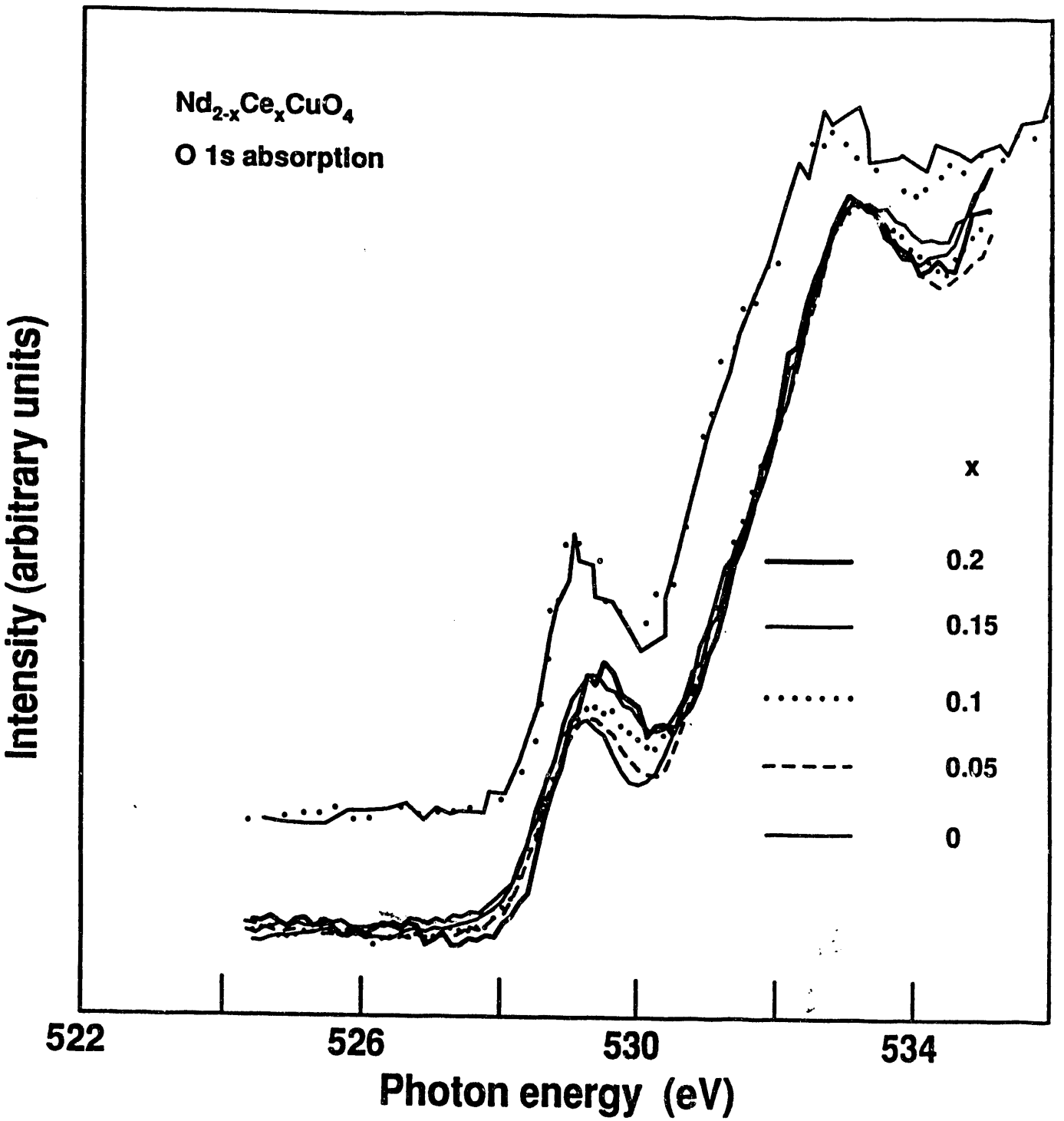
$Nd_{2-x}Ce_xCuO_4$
O 1s absorption
Intensity (arbitrary units)
x
0.2
0.15
0.1
0.05
0
522
526
530
534
Photon energy (eV)

Fig. 15

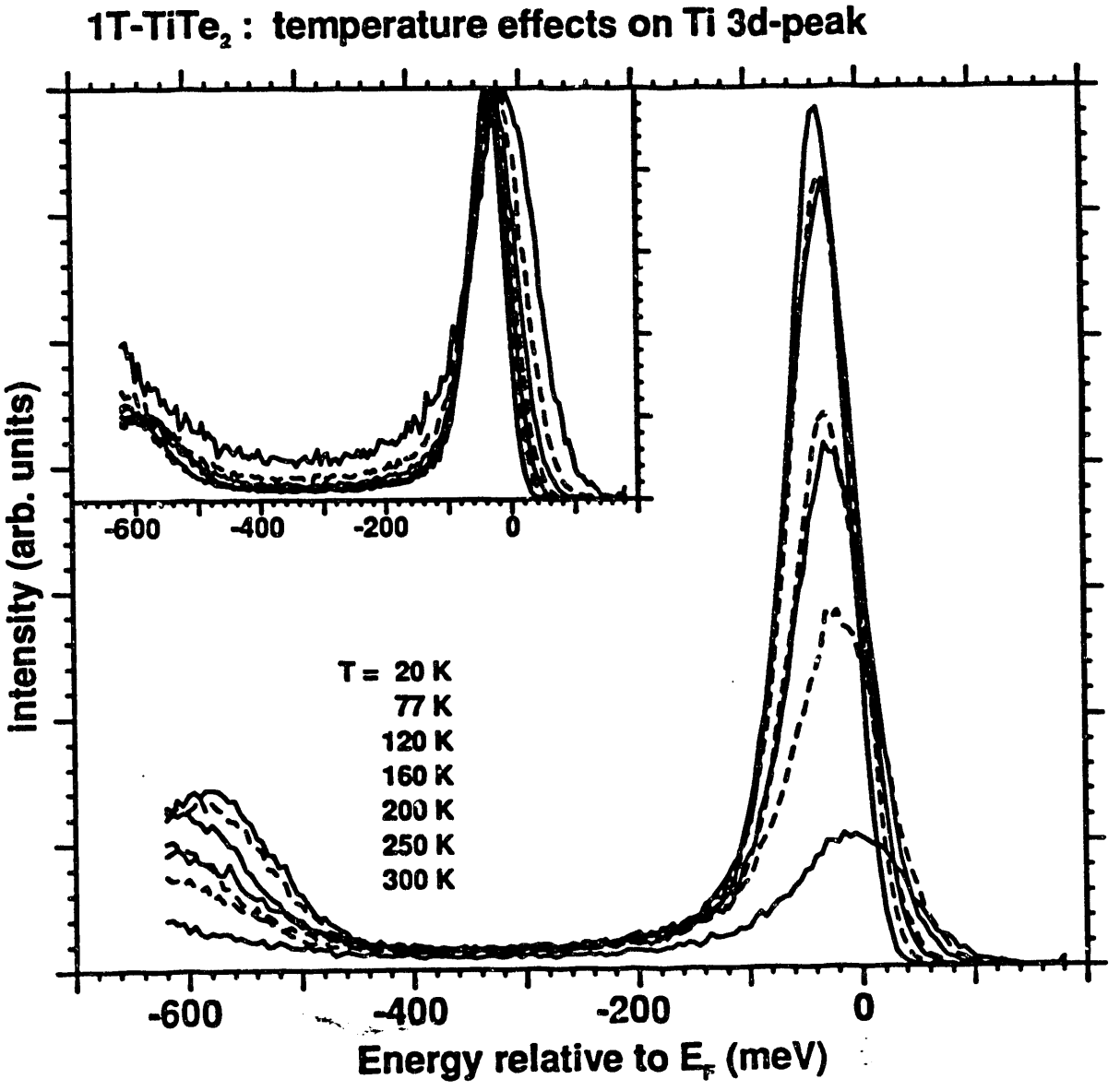
1T-TiTe2 : temperature effects on Ti 3d-peak
Intensity (arb. units)
T = 20 K
77 K
120 K
160 K
200 K
250 K
300 K
-600
-400
-200
0
Energy relative to EF (meV)

Fig. 16

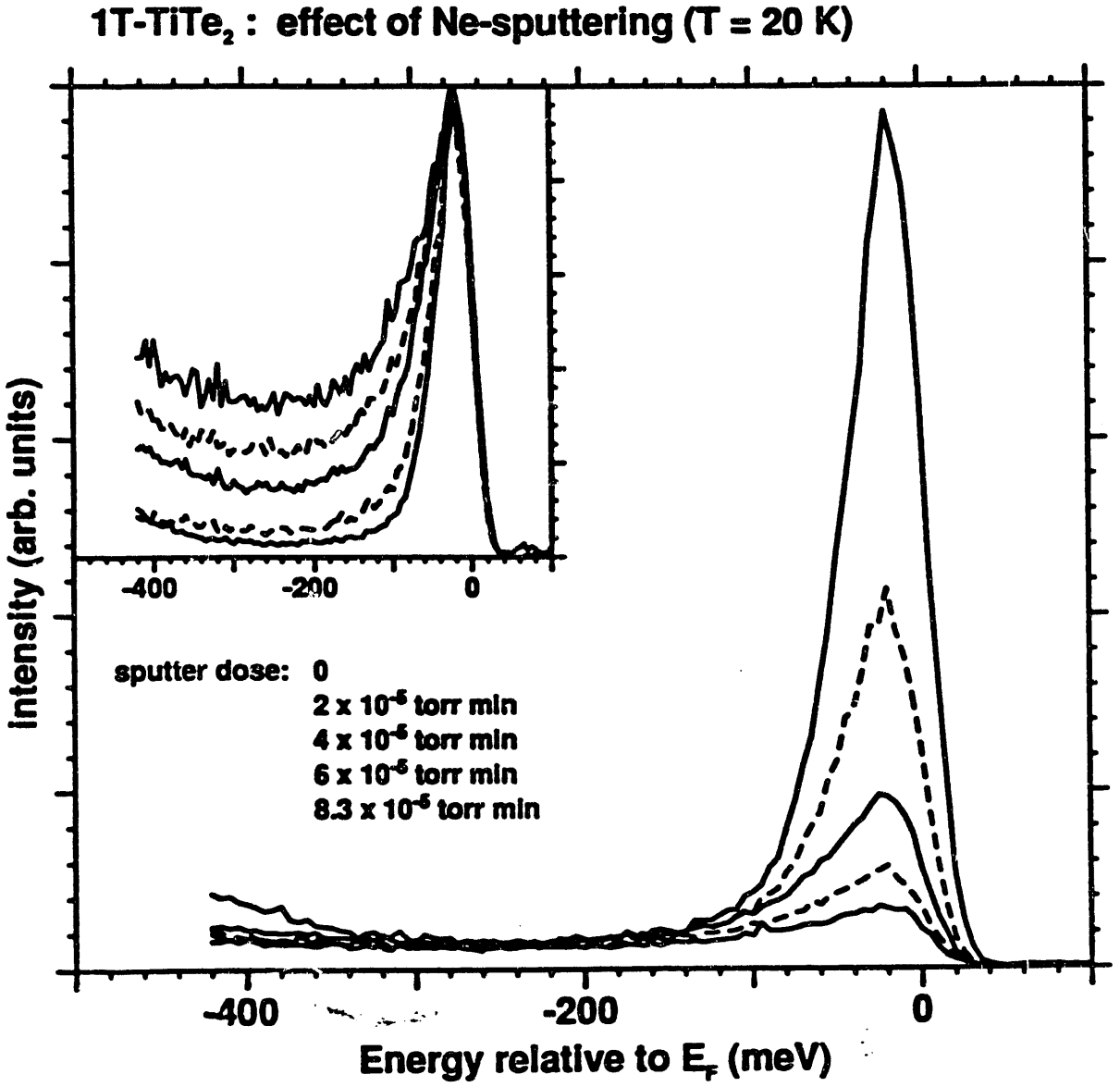
1T-TiTe2 : effect of Ne-sputtering (T = 20 K)
Intensity (arb. units)
-400
-200
0
sputter dose: 0
2 x 10-5 torr min
4 x 10-5 torr min
6 x 10-5 torr min
8.3 x 10-5 torr min
-400
-200
0
Energy relative to EF (meV)

Fig. 17

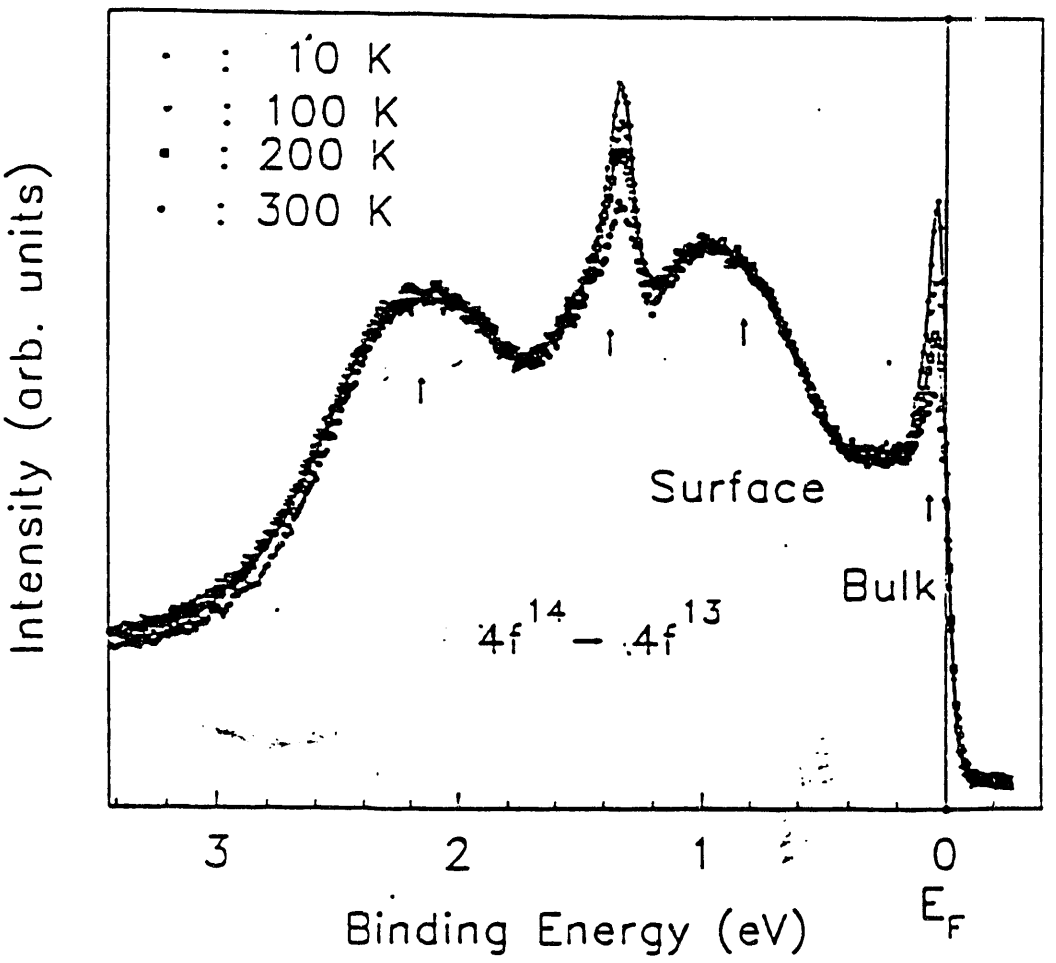
10 K
100 K
200 K
300 K
Intensity (arb. units)
Surface
Bulk
$4f^{14} - 4f^{13}$
3
2
1
0
E_F
Binding Energy (eV)

Fig. 18

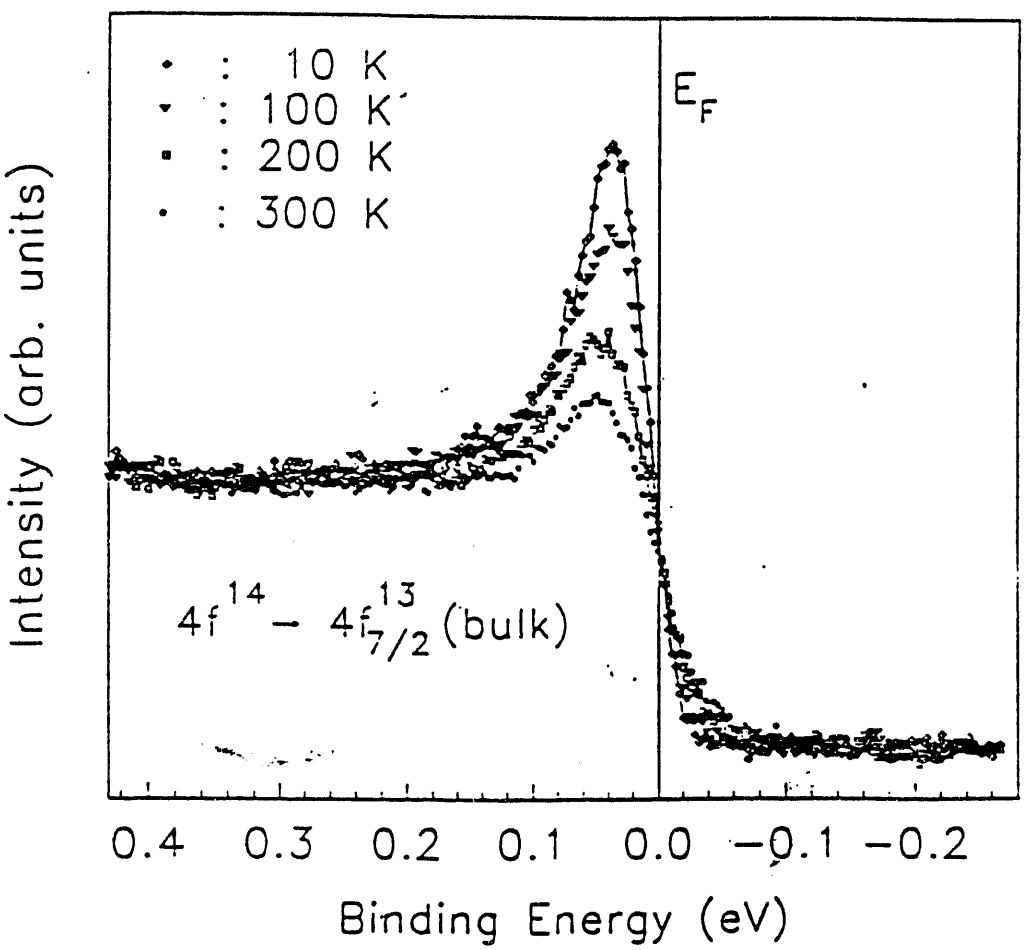
• : 10 K
• : 100 K
• : 200 K
• : 300 K
E_F
$4f^{14} - 4f^{13}_{7/2}$ (bulk)
Intensity (arb. units)
0.4 0.3 0.2 0.1 0.0 −0.1 −0.2
Binding Energy (eV)

Fig. 19

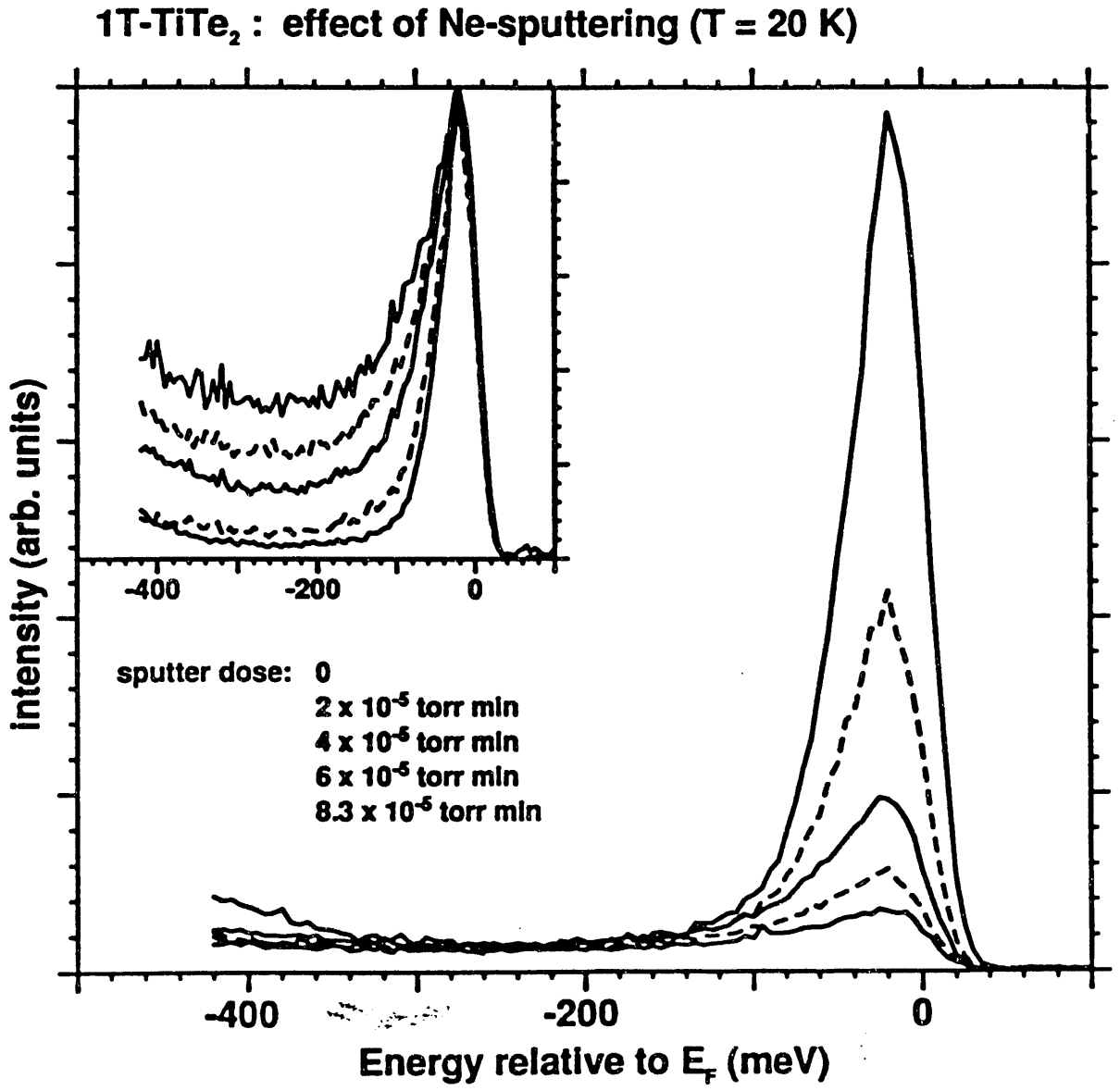
1T-TiTe2 : effect of Ne-sputtering (T = 20 K)
Intensity (arb. units)
-400
-200
0
sputter dose: 0
2 x 10-5 torr min
4 x 10-5 torr min
6 x 10-5 torr min
8.3 x 10-5 torr min
-400
-200
0
Energy relative to EF (meV)

Fig. 17

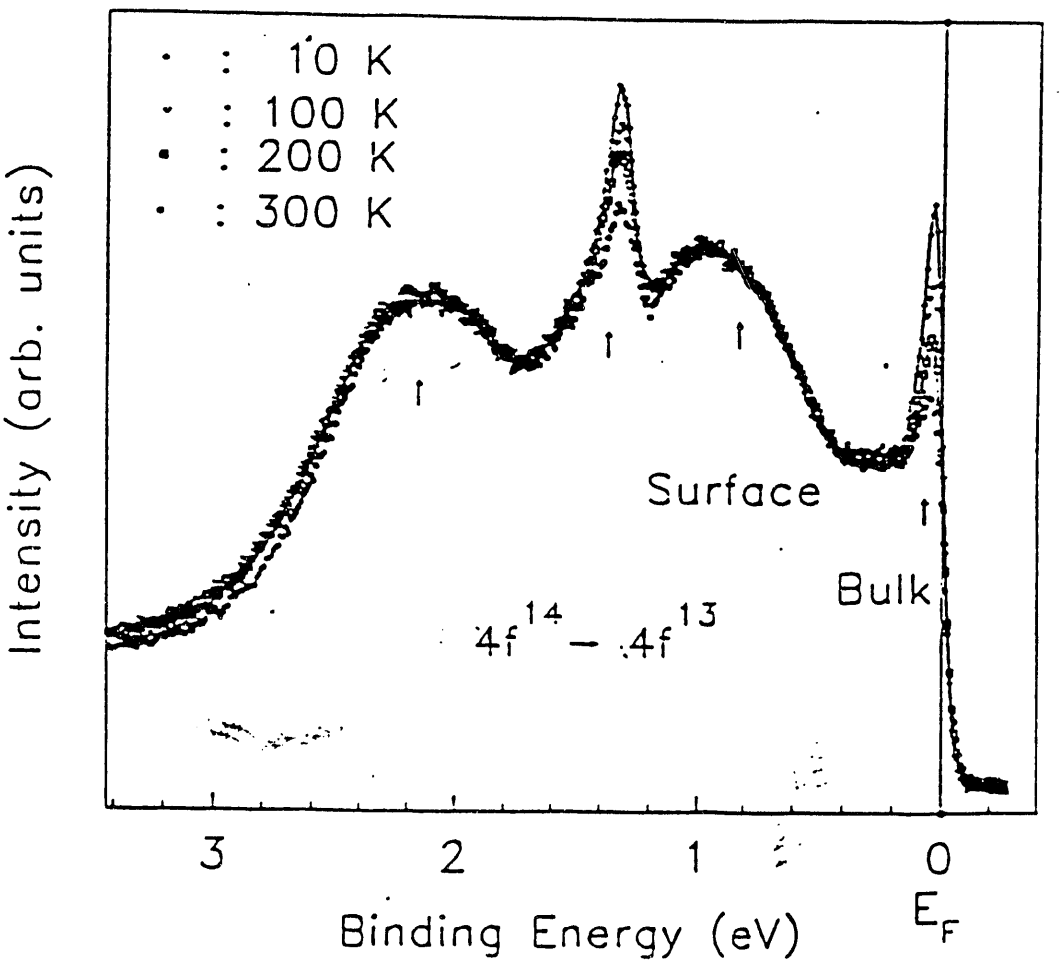
10 K
100 K
200 K
300 K
Intensity (arb. units)
Surface
Bulk
$4f^{14} - 4f^{13}$
3
2
1
0
E_F
Binding Energy (eV)

Fig. 18

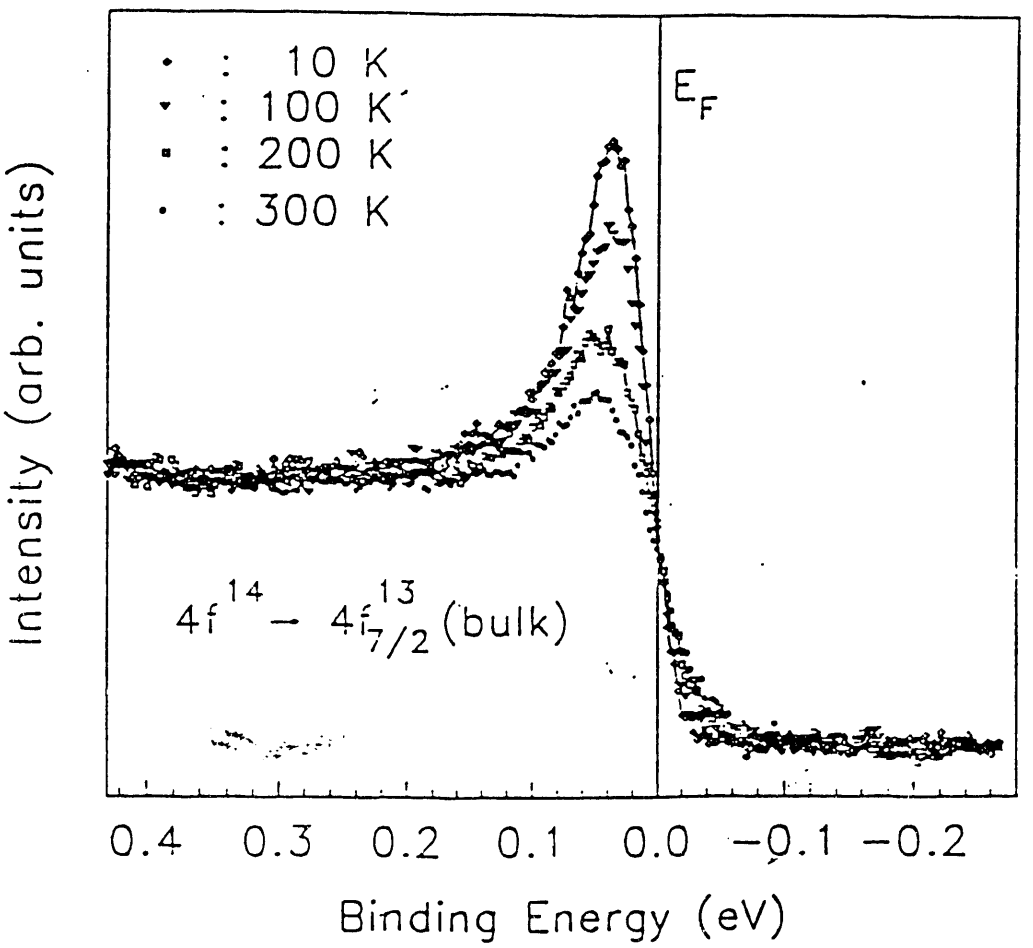
10 K
100 K
200 K
300 K
E_F
Intensity (arb. units)
$4f^{14} \rightarrow 4f^{13}_{7/2}$ (bulk)
0.4
0.3
0.2
0.1
0.0
−0.1
−0.2
Binding Energy (eV)

Fig. 19

END

DATE
FILMED
3/9/93